

1      Proposal for a Full-Scale Detector Engineering Test  
2      and Test Beam Calibration of a Single-Phase LAr  
3      TPC

4      A. name<sup>1</sup>, B. name<sup>2</sup>, and C. name<sup>3</sup>

5      <sup>1</sup>Department of X1, University Y1

6      <sup>2</sup>Department of X2, University Y2

7      <sup>3</sup>Department of X3, University YY3

8      April 15, 2015

9      **Abstract**

10     After a short introduction to the DUNE physics program we motivate the pro-  
11     posed single phase liquid argon detector and charged particle beam measurement  
12     program. We describe the required beam line and beam monitoring instrumen-  
13     tation for the project. The proposed single phase liquid argon detector presently  
14     described corresponds to the LBNE detector design. Discussions about alternate  
15     designs are in progress and this proposal will be updated according to a developing  
16     consensus on the detector design. The detector will be placed inside a membrane  
17     cryostat which will be connected to a cryogenics systems for which we provide  
18     engineering details. The proposal concludes with a description of data handling  
19     and analysis plans, as well as a schedule and an overview of the organizational  
20     structure put in place to execute the plan.

# 21 Contents

22	<b>1 Introduction</b> [~5 pages; <b>Thomas/Greg/B.Wilson</b> ]	3
23	1.1 Key physics goals of ELBNF . . . . .	4
24	1.2 Single-phase LAr detector . . . . .	4
25	1.3 Goals for the prototype detector and beam test . . . . .	5
26	<b>2 CERN prototype detector and charged particle beam test</b> [~10 pages; <b>Donna/Jarek</b> ]	6
27	2.1 Requirements for the detector, beam and commissioning . . . . .	7
28	2.2 Detector performance tests . . . . .	11
29	2.3 Other measurements . . . . .	13
31	<b>3 Single Phase LAr Detector</b> [~10 pages; <b>J. Stewart et al.</b> ]	14
32	3.1 ELBNF detector . . . . .	14
33	3.2 CERN prototype detector . . . . .	15
34	<b>4 Cryostat and cryogenics system</b> [~5 pages; <b>David/Barry/Jack</b> ]	29
35	4.1 Cryostat . . . . .	29
36	4.2 Cryostat size from TPC dimensions (Move to begining of sec 4 per DM)	37
37	4.3 Cryogenic System . . . . .	39
38	<b>5 Charged Particle Test Beam Requirements</b> [~10 pages; <b>Cheng-Ju</b> ]	42
39	5.1 Particle Beam Requirements . . . . .	42
40	5.2 EHN1 H4ext Beamlne . . . . .	43
41	5.3 Beam Instrumentation . . . . .	43
42	5.4 Beam Window on LAr Cryostat . . . . .	45
43	<b>6 Computing requirements, data handling and software</b> [~3 pages; <b>Maxim/Craig</b> ]	45
44	6.1 Collecting and Storing Raw Data . . . . .	46
45	6.2 Databases . . . . .	48
46	6.3 A note on Simulation and Reconstruction Software . . . . .	48
47	6.4 Distributed Computing, Workload and Workflow Management . . . . .	49
48	<b>7 CERN neutrino platform test environment</b> [5 pages; <b>David/Jack/Cheng-Ju/Thomas</b> ]	50
50	<b>8 Schedule, organization and cost estimate</b> [~5 pages; <b>Thomas/Greg</b> ]	51
51	8.1 Schedule . . . . .	51
52	8.2 Organization . . . . .	51
53	8.3 Division of Responsibilities . . . . .	52
54	<b>9 Summary</b> [~2 pages; <b>Thomas/Greg</b> ]	52

## 55 1 Introduction [~5 pages; Thomas/Greg/B.Wilson]

56 The preponderance of matter over antimatter in the early Universe, the dynamics of  
57 the supernova bursts that produced the heavy elements necessary for life and whether  
58 protons eventually decay - these mysteries at the forefront of particle physics and astro-  
59 physics are key to understanding the early evolution of our Universe, its current state  
60 and its eventual fate. The Experiment at the Long-Baseline Neutrino Facility (ELBNF)  
61 represents an extensively developed plan for a world-class experiment dedicated to ad-  
62 dressing these questions.

63 Experiments carried out over the past half century have revealed that neutrinos  
64 are found in three states, or flavors, and can transform from one flavor into another.  
65 These results indicate that each neutrino flavor state is a mixture of three different  
66 nonzero mass states, and to date offer the most compelling evidence for physics beyond  
67 the Standard Model. In a single experiment, ELBNF will enable a broad exploration  
68 of the three-flavor model of neutrino physics with unprecedented detail. Chief among  
69 its potential discoveries is that of matter-antimatter asymmetries (through the mech-  
70 anism of charge-parity violation) in neutrino flavor mixing - a step toward unraveling  
71 the mystery of matter generation in the early Universe. Independently, determination  
72 of the unknown neutrino mass ordering and precise measurement of neutrino mixing  
73 parameters by ELBNF may reveal new fundamental symmetries of Nature.

74 Grand Unified Theories, which attempt to describe the unification of the known  
75 forces, predict rates for proton decay that cover a range directly accessible with the next  
76 generation of large underground detectors such as the ELBNF detector. The experi-  
77 ment's sensitivity to key proton decay channels will offer unique opportunities for the  
78 ground-breaking discovery of this phenomenon.

79 Neutrinos emitted in the first few seconds of a core-collapse supernova carry with  
80 them the potential for great insight into the evolution of the Universe. ELBNF's capa-  
81 bility to collect and analyze this high-statistics neutrino signal from a supernova within  
82 our galaxy would provide a rare opportunity to peer inside a newly-formed neutron star  
83 and potentially witness the birth of a black hole.

84 To achieve its goals, ELBNF is centered around three central components: (1) a  
85 new, high-intensity neutrino source generated from a megawatt-class proton accelerator  
86 at Fermi National Accelerator Laboratory (Fermilab), (2) a fine-grained near neutrino  
87 detector installed just downstream of the source, and (3) a massive liquid argon (LAr)  
88 time-projection chamber (TPC) deployed as a far detector deep underground at the  
89 Sanford Underground Research Facility (SURF). This facility, located at the site of the  
90 former Homestake Mine in Lead, South Dakota, is  $\sim$ 1,300 km from the neutrino source  
91 at Fermilab - a distance (baseline) that delivers optimal sensitivity to neutrino charge-  
92 parity symmetry violation and mass ordering effects. This ambitious yet cost-effective  
93 design incorporates scalability and flexibility and can accommodate a variety of upgrades  
94 and contributions.

95 ELBNF plans to place modular LAr TPCs with a combined total fiducial mass of at  
96 least 40 kton in the underground facility at Homestake and into the neutrino beam. The  
97 first 10 kton LAr TPC module is planned to be constructed underground on the time  
98 scale of 2021.

99 With its exceptional combination of experimental configuration, technical capabili-

ties, and potential for transformative discoveries, ELBNF promises to be a vital facility for the field of particle physics worldwide, providing physicists from institutions around the globe with opportunities to collaborate in a twenty to thirty year program of exciting science.

## 1.1 Key physics goals of ELBNF

The primary goal of ELBNF is to measure the appearance of electron neutrinos in a beam of muon neutrinos and the appearance of electron anti-neutrinos in a beam of muon anti-neutrinos, each over the 1300 km baseline of the experiment. Precise measurement of this phenomenon would allow for determination of the relative masses and mass ordering of the three known neutrinos. Measurement of these neutrino oscillation channels also allow to constrain or measure the CP violation phase,  $\delta_{CP}$  in the neutrino sector, which is possibly connected to the dominance of matter over antimatter in the universe.

For a baseline of 1300 km the first maximum of the oscillation probability occurs in the 2 - 3 GeV energy range with additional oscillation maxima at lower energies. Hence the high intensity neutrino flux must be peaked in this energy range. Coverage of the sub GeV energy range is desirable to potentially map out the second maximum in the oscillation probability. It is this key physics which dictates the neutrino energy range and thereby the energy range of charged particles which result from neutrino interactions in the ELBNF detectors.

## 1.2 Single-phase LAr detector

The basic components of the liquid argon detector include a cryostat and associated cryogenic system. A time projection chamber (TPC) and readout electronics are housed in the cryostat.

The cryostat contains the liquid argon target material and the cryogenic system keeps the liquid argon at a cryogenic temperature of 89K, and maintains the required purity through pump and filter system. A uniform electric field is created within the TPC volume between cathode planes and anode wire planes. Charged particles passing through the TPC release ionization electrons that drift to the anode wires. The bias voltage is set on the anode plane wires so that ionization electrons drift between the first several (induction) planes and is collected on the last (collection) plane. Readout electronics amplify and continuously digitize the induced waveforms on the sensing wires at several MHz, and transmit these data to the DAQ system for analysis. The wire planes are oriented at different angles allowing a 3D reconstruction of the particle trajectories. In addition to these basic components, a photon detection system is also included in the design to enable the study of proton decay and be sensitive to galactic supernova neutrinos.

The LAr detector design is characterized by a modular approach in which the LAr volume in the cryostat is instrumented with a number of identical anode wire plane assemblies (APA) and associated cathode plane assemblies (CPA). To a large extent, scaling from detector volumes containing from a few to several hundred of such modules should be straightforward with small and predictable risk.

### **141 1.3 Goals for the prototype detector and beam test**

142 The physics sensitivity of ELBNF has been estimated based on detector performance  
143 characteristics published in the literature, simulation based estimates as well as a vari-  
144 ety of assumptions about the anticipated performance of the future detector and event  
145 reconstruction and particle identification algorithms. The proposed single phase LAr  
146 prototype detector and CERN beam test aim to replace these assumptions with mea-  
147 surements for the full scale ELBNF detector components and the presently available  
148 algorithms. Thereby the measurements will allow to enhance the accuracy and reliabil-  
149 ity of the ELBNF physics sensitivity projections. The beam measurements will serve  
150 as a calibration data set to tune the Monte Carlo simulations and serve as a reference  
151 data set for measurements of the future ELBNF detector. In addition, the measurement  
152 program aims to evaluate and benchmark the performance of the detector and its indi-  
153 vidual components. This will allow to identify potentially problematic components and  
154 lead to future improvements and optimizations of the detector design.

155 In order to make such precise measurements, the detector will need to accurately  
156 identify and measure the energy of the particles produced in the neutrino interaction  
157 with Argon which will range from hundreds of MeV to several GeV. To mitigate the  
158 risks associated with extrapolating small scale versions of the single-phase LAr TPC  
159 technology to a full-scale detector element, it is essential to benchmark the operation of  
160 a full-scale detector elements in a well characterized charged particle beam.

161 More specifically, the goals of the prototype detector and beam test measurements  
162 include the the use of a charged particle beam to:

- 163 1. measure the detector calorimetric response for
  - 164 (a) hadronic showers
  - 165 (b) electromagnetic showers
- 166 2. study e/ $\gamma$ -separation capabilities
- 167 3. measure event reconstruction efficiencies as function of energy and particle type  
168 based on experimental data
- 169 4. measure performance of particle identification algorithms as function of energy and  
170 for realistic detector conditions
- 171 5. assess single particle track calibration and reconstruction
- 172 6. validate accuracy of Monte Carlo simulations for relevant energy ranges as well as  
173 directions
- 174 7. study other topics with the collected data sets
  - 175 (a) pion interaction kinematics and cross sections
  - 176 (b) kaon interaction cross section to characterize proton decay backgrounds ...
  - 177 (c) muon capture for charge identification

178 For the detector performance characterization a well defined charged particle test  
179 beam will enable the following detector performance measurements:

- 180 1. characterize performance of full scale TPC module
- 181 2. verify functionality of cold TPC electronics under LAr cryogenic conditions
- 182 3. perform full-scale structural test under LAr cryogenic conditions
- 183 4. study performance of the photon detection system
- 184 5. verify argon contamination levels and associated mitigation procedures
- 185 6. develop and test installation procedures for full-scale detector components
- 186 7. test and evaluate the performance of detector calibration tools

187 The CERN charged particle beam lines provide an opportunity to perform this crucial  
188 test of the proposed single-phase LAr TPC and thereby inform the decision regarding  
189 the far detector design and layout for ELBNF. In order to be of greatest value to this  
190 decision making process results should be available as soon as possible.

191 This technical document describes the motivation and technical details for an initial  
192 measurement program that we propose to be executed by mid 2018, that is *before* the  
193 anticipated LHC long shutdown. The estimated required beam time amounts to  $\sim$  XX  
194 weeks of data collection. Additional follow-up measurements with potentially modified  
195 detector components form a potential extension to the proposed program.

## 196 2 CERN prototype detector and charged particle 197 beam test [ $\sim$ 10 pages; **Donna/Jarek**]

### 198 TODO list

199 **Sensitivity plots.** Create plots for the CPV and HM sensitivities for 40kton detector  
200 and 1.2 MW beam. Plots should include various combinations of the assumed  
201 uncertainties: with current best measurements, with best guesses about uncer-  
202 tainties we can archive and with uncertainties which will be obtain using beam  
203 test experiment at CERN.

204 **E-m shower calibration energy scale.** Estimate statistics of particles to optimise  
205 the measurement of EM showers. Provide the necessary statistics as a function of  
206 energy. Optimise the energy bins widths, where we expect coarser bins for higher  
207 energies than for lower energies.

208 **Hadronic shower calibration** Estimate statistics of particles to optimise the mea-  
209 surement of hadronic showers. Provide the necessary statistics as a function of  
210 energy. Optimise the energy bins widths, were we expect coarser bins for higher  
211 energies than for lower energies.

212 Estimate pi0 production from the proton scattering in the TPC.

- 213 **Reconstruction issues.** Obtain values for the uncertainties due to finding vertex po-  
 214 sition of neutrino interactions.  
 215 Estimate statistics necessary to improve low energy electrons acceptance due to  
 216 reconstruction algorithms limitations.  
 217 **e/gamma separation** Estimate statistics necessary for improvement of the e/gamma  
 218 separation. Assume three values for wire pitch: 3mm, 4mm and 5mm.  
 219 **Pion cross sections: absorption, charge exchange in Ar** Get statistics for pions  
 220 to measure their cross sections. Estimate energy bin widths.  
 221 **Kaon cross section in Ar** Get statistics for kaons to measure their cross sections.  
 222 Estimate energy bin widths.  
 223 **Muon capture** Estimate statistics for antimuons for capture on argon to be used for  
 224 the statistical determination of the wrong sign neutrino contribution on the beam.

## 225 2.1 Requirements for the detector, beam and commissioning

226 The Single-Phase Cern Prototype detector is intended to provide necessary information  
 227 to reduce systematic uncertainties for the oscillation measurements in the US-based  
 228 long base-line neutrino experiment. The LAr TPC technology is not new but wasn't  
 229 extensively used in the 1-10 GeV neutrino energy range. The main source of uncertainties  
 230 due to detector with the current values are shown in table 1

Table 1: Current known sources of detector uncertainties for liquid argon or TPC.

source of uncertainty	value	reference
e/ $\gamma$ separation		
e-m shower calibration		
hadronic shower calibration		
low energy acceptance electron identification		
.....		

Table 2: Current known sources of uncertainties due to interaction of charged particle with argon.

source of uncertainty	value	reference
pion(Kaon) absorbtion		
pion(Kaon) charge exchange		
pion (Kaon) production in secondary interactions		
muon capture	Phys. Rev. C 35, 2212	
energy scale		
Michel electron tagging		
.....		

231 With current detector uncertainties from table 1 the sensitivities for the CP violation  
232 phase measurement is shown in Fig. 2.1 **Task: make this plot**. The proposed test  
233 beam detector will reduce uncertainties to XX% and improve our sensitivity to  $\delta_{CP}$  as  
234 shown in Fig. 2.1 **Task: make this plot**.

Figure 1: Sensitivities for the  $\delta_{CP}$  measurement for using current knowledge of the single-phase LAr-TPC detector technology and for reduced detector uncertainties from SPCP beamtest data. The plots prepared for 40 kton fiducial mass and  $xx \times 10^{21}$ POT.

235 **2.1.1 Particles energy and direction**

236 Plans for running beam for the the ELBNF include both neutrino and anti-neutrino  
237 configurations. These beams will be composed mainly of muon neutrinos (anti-neutrinos)  
238 as well as electron neutrinos (anti-neutrinos). In figures 2.1.1 and 2.1.1 the distributions  
239 on momenta and angles of particles created in neutrino interaction are shown.

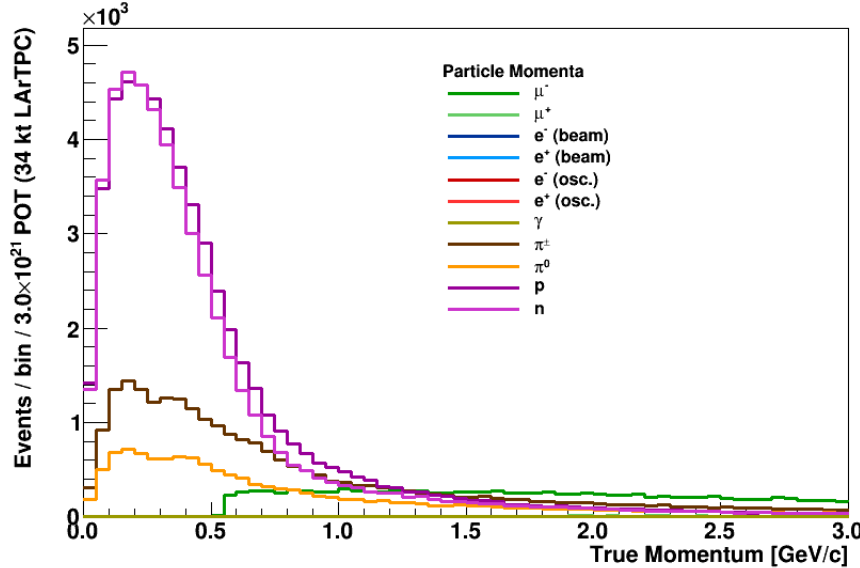


Figure 2: Particle momenta distributions for particles coming from all fluxes ( $\nu_e$ ,  $\nu_\mu$ ,  $\bar{\nu}_e$  and  $\bar{\nu}_\mu$ ) at both near and far detector locations.

Figure 3: Particle angle wrt to the beam axis distributions for particles coming from all fluxes ( $\nu_e$ ,  $\nu_\mu$ ,  $\bar{\nu}_e$  and  $\bar{\nu}_\mu$ ) at both near and far detector locations.

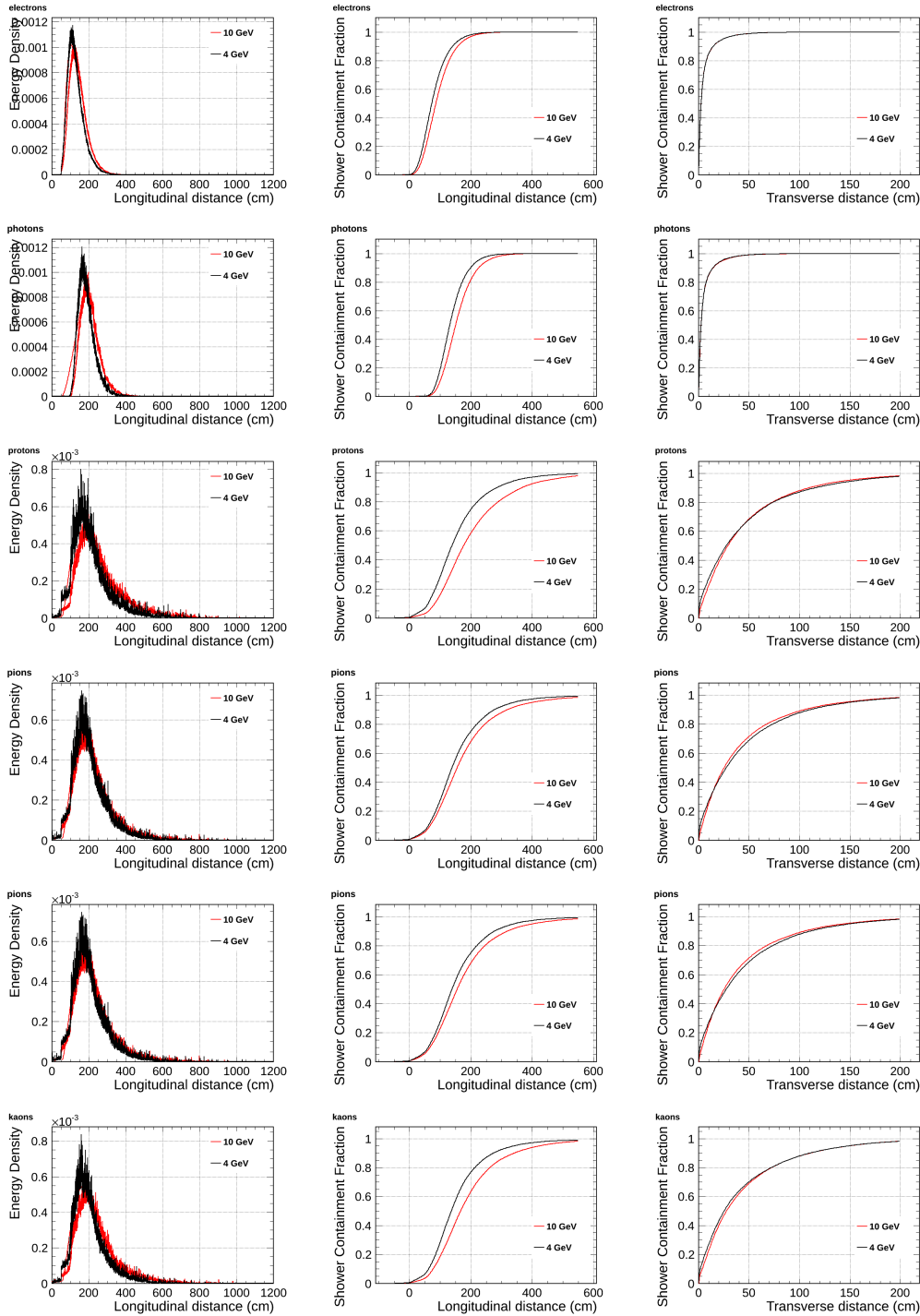


Figure 4: Particle containment plots.

<sup>240</sup> **2.1.2 Run plan**

Table ?? summarizes the required exposures to beam particles.

Particle	Momenta (GeV)	Exposure	Purpose
$\pi^+$	0.2, 0.3, 0.4, 0.5, 0.7, 1, 2, 3, 5, 7	10K	hadronic cal, $\pi^0$ content
$\pi^+$	1	2M	$\pi^0/\gamma$ sample
$\pi^-$	0.2, 0.3, 0.4, 0.5, 0.7, 1	10K	hadronic cal, $\pi^0$ content
$e^+$ or $e^-$	0.2, 0.3, 0.4, 0.5, 1, 2, 3, 5, 7	10K	$e-\gamma$ separation/EM shower
$\mu^-$	(0.2), 0.5, 1, 2	10K	$E_\mu$ , Michel el., charge sign
$\mu^+$	(0.2), 0.5, 1, 2	10K	$E_\mu$ , Michel el., charge sign
$\mu^-$ or $\mu^+$	0.5, 1, 2, 5, 7	5K	$E_\mu$ MCS
proton	0.2, 0.3, 0.5, 0.7, 1, 2, 3	10K	response, PID
proton	1	(2M)	mis-ID pdk
antiproton	low-energy tune	(100)	antiproton stars
$K^+$	1	(13k)	response, PID, pdk
$K^+$	0.5, 0.7	(5k)	response, PID, pdk

Table 3: Requirements summary for nominal beam direction. Items in parenthesis indicate somewhat lower priority (see text).

<sup>241</sup>

<sup>242</sup> **2.2 Detector performance tests**

<sup>243</sup> **2.2.1 Bethe-Bloch parametrisation of charged particles**

<sup>244</sup> The prototype detector will allow to study the detector response to charge particles from  
<sup>245</sup> the test beam and will serve as a calibration detector. The measured energy deposition  
<sup>246</sup> for various particles and its dependence on the direction of the particle will feed into  
<sup>247</sup> our Monte Carlo generator and allow more precise reconstruction of neutrino energy and  
<sup>248</sup> interactions topologies with good particle identifications.

<sup>249</sup> **How we compare with Lariat? Multiple scattering**

<sup>250</sup> The set of single-phase prototype detector helped to understand the detector response  
<sup>251</sup> to cosmic muons. But there is still lots to learn with additional studies. The charge  
<sup>252</sup> particle identification efficiencies has been mapped for only limited range of the particle  
<sup>253</sup> energies.

<sup>254</sup> **2.2.2  $e/\gamma$  separation**

<sup>255</sup> The search for a CP violation phase using  $\nu_e$  appearance in a  $\nu_\mu$  beam requires good  
<sup>256</sup> electron/photon separation. Backgrounds originating from photons produced primarily  
<sup>257</sup> from final state  $\pi^0$ 's must be identified and removed from the signal electron sample.

<sup>258</sup> The photons can undergo two process: pair production and Compton scattering. The  
<sup>259</sup> dominant process for photons with energies of several hundreds MeV is the  $e^+ e^-$  pair  
<sup>260</sup> production, but Compton scattering also occur at this energies. For pair production the  
<sup>261</sup>  $e/\gamma$  separation is achieved by looking at the beginning of the electromagnetic shower,  
<sup>262</sup> where for election we see energy deposition typical for single MIP and for photon we see

263 energy deposition consisted with two MIPs. In case of Compton scattering off of atomic  
264 electrons the signal is much more difficult to distinguish from the CC  $\nu_e$  scattering signal.

265 Electron-photon separation has been studied in LAr TPCs (Icarus and Argoneut)  
266 as shown in Fig. ???. Currently the separation efficiency is estimated to be at the level  
267 of 94 % (? cite and check the number). This may depend on particular features of  
268 the geometry including wire pitch, etc. Therefore, it is critically important to study e/ $\gamma$   
269 separation in a prototype LAr TPC detector. **we need someone to look into this**

### 270 2.2.3 Reconstruction efficiencies and particle identification

271 The reconstruction of events in the LAr TPC is still a challenge but rapid progress has  
272 been achieved in recent years (cite pandora and other reconstruction algorithms). De-  
273 spite the progress reconstruction algorithms have to rely Monte Carlo predictions which  
274 don't simulate liquid argon detectors responses correctly. Reconstruction algorithms  
275 will benefit greatly from test beam data particularly from the full scale prototype. The  
276 reconstruction algorithms will be trained to correctly reconstruct track, electromagnetic  
277 and hadronic showers. The data of tracks and showers can be used to create a library  
278 of reference events with which to tune algorithms.

279 Main issues for the reconstruction algorithms:

- 280 • The reconstruction algorithms try to use all three planes on the signal readout. if  
281 the orientation of the track/shower is such that it is aligned with wires on one of  
282 the plans it significantly reduces quality of reconstructed objects.
- 283 • Calorimetry with collection and induction planes. In the ICARUS experiment the  
284 deposited energy was reconstructed from the signal on the collection plane. The  
285 induction planes bipolar signal wasn't "stable" enough to use it for calorimetric  
286 measurement. In the ELBNF design there is additional shielding wire plane which  
287 will improve the quality of the bipolar signal and the test beam experiment will  
288 help with its calibration.
- 289 • Vertexing.
- 290 • Reconstruction efficiency for low energy particles. The reconstruction algorithm  
291 suffer from the lose of efficiency for low energy particle or particles which leave less  
292 than 200-300 hits. Training the algorithms on a low energy particles from the test  
293 beam will improve the quality and efficiency of the reconstructed objects.

### 294 2.2.4 Cross section measurements

295 Precise measurement of the absorption and charge exchange of pions and kaons. Pion  
296 absorption is a large part of the pion nucleon cross section from 50 MeV to 500MeV with  
297 no data above about 1GeV pion kinetic energy. **Add plots and values for known**  
298 **cross sections wit errors**

- 299 • pion absorption on argon - Kotlinski, EPJ 9, 537 (2000)
- 300 • pion cross section as a function of A - Gianelli PRC 61, 054615 (2000)

301 There is not currently a satisfactory theory describing absorption. The Valencia group  
 302 (Vicente-Vacus NPA 568, 855 (1994)) developed model of the pion-nucleus reaction with  
 303 fairly good agreement, although not in detail. The actual mechanism of multi-nucleon  
 304 absorption is not well understood.

305 **2.2.5 Charge sign determination**

306 It is not possible to determine charge of the particle on the event by event basis with  
 307 non-magnetised LAr TPC detectors. A statistical separation will be studied which will  
 308 make use of differences in muon versus antimuon capture cross sections and lifetime. For  
 309 the  $\mu^+$  for argon we expect about xx% to be captured and for  $\mu^-$  about yy%.

310 **2.2.6 Single track calibration**

311 **2.2.7 Shower calibration**

312 Reconstruction of neutrino energy depends of a quality of reconstruction of both elec-  
 313 tromagnetic and hadronic showers.

314 - features of Hadronic shower in LAr TPC - features of electromagnetic  
 315 shower in LAr TPC - Missing energy from neutral (Neutrons scattering)

316 **2.3 Other measurements**

317 **2.3.1 Anti-proton annihilation**

318 **2.3.2 Proton decay background (cosmogenic  $K^0 \rightarrow K^+$ )**

Particle	Momenta (GeV)	Exposure/bin (total)
$K^+$	0.5-0.8 MeV (50 MeV bins)	1000 (6k)
$K^-$	0.5-0.8 MeV (50 MeV bins)	1000 (6k)

Table 4: Data sample requirements for calibrate absolute energy scale.

319 **2.3.3 Supernova**

320 The energies of the electrons coming from CC  $\nu_e$  interactions from Supernova will be in  
 321 the order of few MeV. The beam test cannot offer such low energy electron, but one  
 322 can use the Michel electrons form ' $\mu$ ' decay to cover these energies. The SK used the  
 323 Michel spectrum to calibrate the absolute energy scale.

Particle	Momenta (GeV)	Exposure/bin (total)
$\mu^+$	any, but need to stop	2000 (2k)

Table 5: Data sample requirements for calibrate absolute energy scale.

324 **3 Single Phase LAr Detector [~10 pages; J. Stewart**  
325 **et al.]**

326 **3.1 ELBNF detector**

327 The far detector for the ELBNF collaboration will be a series of four liquid argon time  
328 projection chambers (TPC), each in a cryostat that holds a fiducial/active/total LAr  
329 mass of 10.0/13.3/16.9 kt. The TPCs will be instrumented with photon detection. It is  
330 planned that the first 10 kt detector will be ready for installation in the 2021 timeframe.  
331 One option for the TPC design is a wire plane based TPC with cold electronics readout.  
332 Designs of this style are referred to as single-phase detectors as the charge genera-  
333 tion, drift, and detection all occurs in the argon liquid phase. This style TPC has the  
334 advantage that there is no charge amplification before collection making a very precise  
335 charge measurement possible. To achieve ELBNF's goals, a detector much larger than  
336 ICARUS, the largest LAr TPC detector built to date, is needed. The LBNE experiment  
337 was developing a scalable far detector design shown in Figure 5 that would scale-up LAr  
338 TPC technology by roughly a factor of 40 compared to the ICARUS T600 detector.  
339 To achieve this scale-up, a number of novel design elements need to be employed. A  
340 membrane cryostat typical for the liquefied natural gas industry will be used instead of  
341 a conventional evacuated cryostat. The wire planes or anode plane assemblies (APAs)  
342 will be factory-built as planar modules that are then installed into the cryostat. The  
343 modular nature of the APAs allow the size of the detector to be scaled up to at least  
344 40 kt fiducial mass. Both the analog and digital electronics will be mounted on the wire  
345 planes inside the cryostat in order to reduce the electronic noise, to avoid transporting  
346 analog signals large distances, and to reduce the number of cables that penetrate the  
347 cryostat. The scintillation photon detectors will employ light collection paddles to re-  
348 duce the required photo-cathode area. Many of the aspects of the design will be tested  
349 in a small scale prototype at Fermilab but given the very large scale of the detector el-  
350 ements a full-scale test is highly desirable. As the new ELBNF collaboration forms and  
351 organized a combined detector design team will emerge. Ideas from this new collabora-  
352 tion will modify the design presented here but this design provides a concrete example  
353 of a possible future detector.

354 The goals of the ELBNE detector test can be broken into four categories: argon  
355 contamination mitigation verification, TPC mechanical verification, TPC electrical veri-  
356 fication, and photon detection light yield verification. Research at Fermilab utilizing the  
357 Materials Test Stand has shown that electronegative contamination to the ultra-pure  
358 argon from all materials tested is negligible if the material is under the liquid argon.  
359 This implies that the dominant source of contamination originates from the gas ullage  
360 region and in the room temperature connections to the detector. Careful design of the  
361 ullage region to insure that all surfaces and feedthroughs are cold is expected to greatly  
362 reduce the sources of contamination over what exists in present detectors. Other con-  
363 cepts attempt to eliminate the gas ullage completely. The goals related to mechanical  
364 testing are to test the integrity of the detector. In the current design, each APA mea-  
365 sures 2.3 m by 6.0 m and includes 2560 wires and associated readout channels. Given  
366 the complexity of these assemblies, a test where the detector can be thermally cycled  
367 and tested under operating conditions is highly advised prior to mass production. The

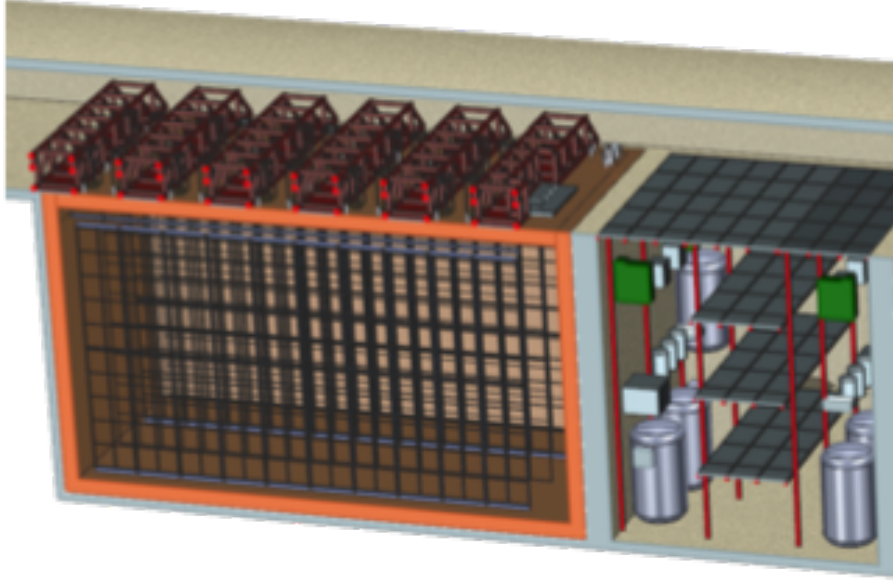


Figure 5: 3D model of one design of the ELBNF single-phase detector. Shown is 5kt fiducial volume detector which would need to be lengthened for the 10 kt design. The present ELBNF plan calls for the construction of 4 10 kt detectors of similar design.

368 mechanical support of the APAs can be tested to verify that the mechanical design is  
 369 reliable and will accommodate any necessary motion between the large wire planes. The  
 370 impact of vibration isolation between the cryostat roof and the detector can also be  
 371 tested. Finally a potential improvement in the cryostat design is the possibility to move  
 372 the pumps external to the main cryostat. This will reduce any mechanical coupling to  
 373 the detector and also greatly improve both reliability and ease of repair. The electrical  
 374 testing goals are to insure that the high voltage design is robust and that the required  
 375 low electronic noise level can be achieved. As the detector scale increases so does the  
 376 capacitance and the stored energy in the device. The design of the field cage and high  
 377 voltage cathode planes needs to be such that HV discharge is unlikely and that if the  
 378 event occurs no damage to the detector or cryostat results. The grounding and shielding  
 379 of large detectors is also critical for low noise operation. By testing the full scale ele-  
 380 ments one insures that the grounding plan is fully developed and effective. Large scale  
 381 tests of the resulting design will verify the electrical model of the detector.

### 382 3.2 CERN prototype detector

#### 383 3.2.1 Overview of the CERN Single-Phase test Detector

384 This sections presents the design details of a single-phase detector based on the de-  
 385 velopment of the LBNE collaboration. As ELBNF moves forward the TPC working  
 386 group will evaluate this and any modifications or alternate proposals. For the purpose  
 387 of this proposal this represents one alternate, and it is expected to evolve as the new  
 388 collaboration organized and more work is done.

389 This TPC consists of alternating anode plane assemblies (APAs) and cathode plane

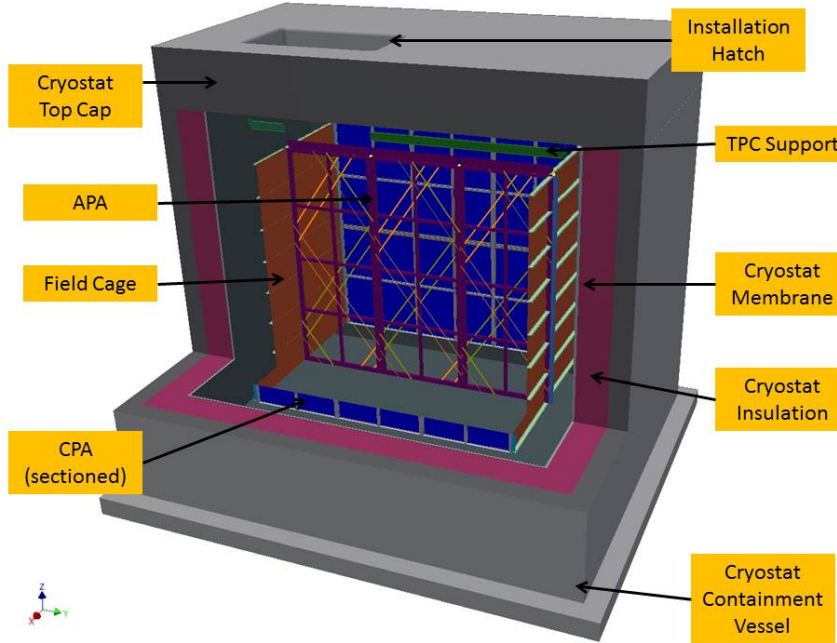


Figure 6: 3D model of the single-phase detector prototype is shown inside the test cryostat.

390 assemblies (CPAs), with field-cage panels enclosing the four open sides between the  
 391 anode and cathode planes. Figure 6 shows a sectioned view for the planned TPC inside  
 392 the cryostat at CERN. A uniform electric field is created in the volume between the anode  
 393 and cathode planes. A charged particle traversing this volume leaves a trail of ionization.  
 394 The electrons drift toward the anode plane, which is constructed from multiple layers of  
 395 sense wires, inducing electric current signals in the front-end electronic circuits connected  
 396 to the wires.

397 To the extent possible the TPC will be assembled from elements that are of the  
 398 same size as those planned for the single phase far detector. The primary exception to  
 399 this is the length of the field cage panels which are 2.5m in this design, compared to  
 400 3.4m in the far detector. This is because the drift distance between the APA and CPA is  
 401 reduced to lessen the impact of space charge on the prototype necessitated by the surface  
 402 operation. The overall size of the TPC will be derived by the size and number of anode  
 403 planes (APA). It has been determined in order to perform the required physics, the TPC  
 404 will have a 3-APA wide active volume. The APAs will have an active (total) area 2.29 m  
 405 (2.32 m) wide and 6.0 m (6.2 m) high. The combination of the three APAs determines  
 406 the overall TPC length to be 7.2 m. There will be a cathode plane (CPA) on either side  
 407 of the APAs. The overall width of the TPC will be determined by a combination of the  
 408 drift distances along with the thickness of the APA, which is constructed of 76.2 x 101.6  
 409 mm stainless steel (SS) structural tubing. The overall width of the TPC is 5.2 m. Like  
 410 the length of the TPC, the overall height will be determined by the height of the APA  
 411 which is 6.3 m. In summary the external TPC dimensions will be 7.2 m long x 5.2 m  
 412 wide x 6.3 m high. Along with the APAs and CPAs, the TPC will include a field cage  
 413 that surrounds the entire assembly. This is a series of pultruded fiberglass I beams for  
 414 the structural elements. These I-beams will be tiled with large copper sided FR4 panels

415 to create the field cage. Each panel will be connected with a series of resistors. The field  
416 cage will be connected to the CPAs through a capacitor assembly.

417 All of this will be supported by rows of I-beams supported from a mechanical struc-  
418 ture above the cryostat. The hangers for these I-beams will pass through the insulated  
419 top cap. There will be a series of feed thru flanges in the top cap of the cryostat to bring  
420 in and take out services for the TPC. There will be a HV feed thru for each of the CPA  
421 rows and one signal feed thru for each of the APAs.

422 The minimum internal size of the cryostat is 9.5 m long, 7.3 m wide and 8.4 m high.  
423 This is determined from size of the TPC. These dimensions also preserve the ability to  
424 reverse the order of the APAs and CPAs inside the TPC. The current plan is to have  
425 the APAs located in the center of the cryostat with a CPA on each side. Reversing this  
426 to have the CPA in the center and APAs on each side may be required to minimize the  
427 dead space between the two drift volumes.

### 428 3.2.2 Anode Plane Assemblies (APAs)

429 Each APA (Figure 7) is instrumented with 3 layers of signal wires, one longitudinal  
430 collection plane and two 35.7° angled induction planes with an additional outer grid plane  
431 that helps maintain the field. The overall dimensions of the active area as mentioned  
432 above are 2.3 m wide, 6 m long. The dimension of the wire planes were selected to fit down  
433 the Ross shaft at SURF, be compatible with a standard HiCube transport container,  
434 and allow construction from readily available materials. The angled layers start at the  
435 electronics end and wind around to the other side on their way to the bottom. The wire  
436 angle was selected so that a given angled induction wire will not overlay any longitudinal  
437 collection wire more than once in order to reduce ambiguities caused by the wrapped  
438 wire construction. Partial wire layers are shown here in Figure 7 at the bottom. With  
439 a wire pitches of 4.67 mm (diagonal layers) and 4.79 (straight layers), the total number  
440 of readout channels in an APA is 2560. The grid layer is not depicted in Figure 7 for  
441 clarity. The underlying structure of each APA is a framework of rectangular, stainless  
442 steel tubing. The side and bottom edges of the frame are lined with multiple layers of  
443 fiberglass circuit boards, notched along the edges to support and locate the wires that  
444 cross the APA face. A set of FR4 combs are glued to the APA frame to capture the  
445 wires at regular intervals. The front-end electronics boards are mounted at the top end  
446 of the frame and protected by a metal enclosure.

447 The distance between wire planes is 4.8 mm (3/16 in) corresponding with standard  
448 printed circuit board thickness, and while maintaining optimal signal formation. The  
449 four wire planes will be electrically biased so that electrons from an ionizing-particle  
450 track completely drift past the first three planes and are collected by the fourth plane.  
451 Calculations show that the minimum bias voltages needed to achieve this goal are  $V_G$   
452 = -665V,  $V_U$  = -370V,  $V_V$  = 0V and  $V_X$  = 820V respectively (where G, U, V, and X  
453 are the wire-layer labels from outside in, towards the frame). It is convenient to set  
454 one of the wire planes to ground so that the wires can be DC coupled to the front-end  
455 readout electronics. In this instance, the V wire plane is set to ground potential to  
456 reduce the maximum bias voltages on the other wire planes, and enable the use of lower  
457 voltage rated AC coupling capacitors. A grounded mesh plane, located 4.8 mm behind  
458 the collection (X) plane, prevents the electric field around this set of wires from being

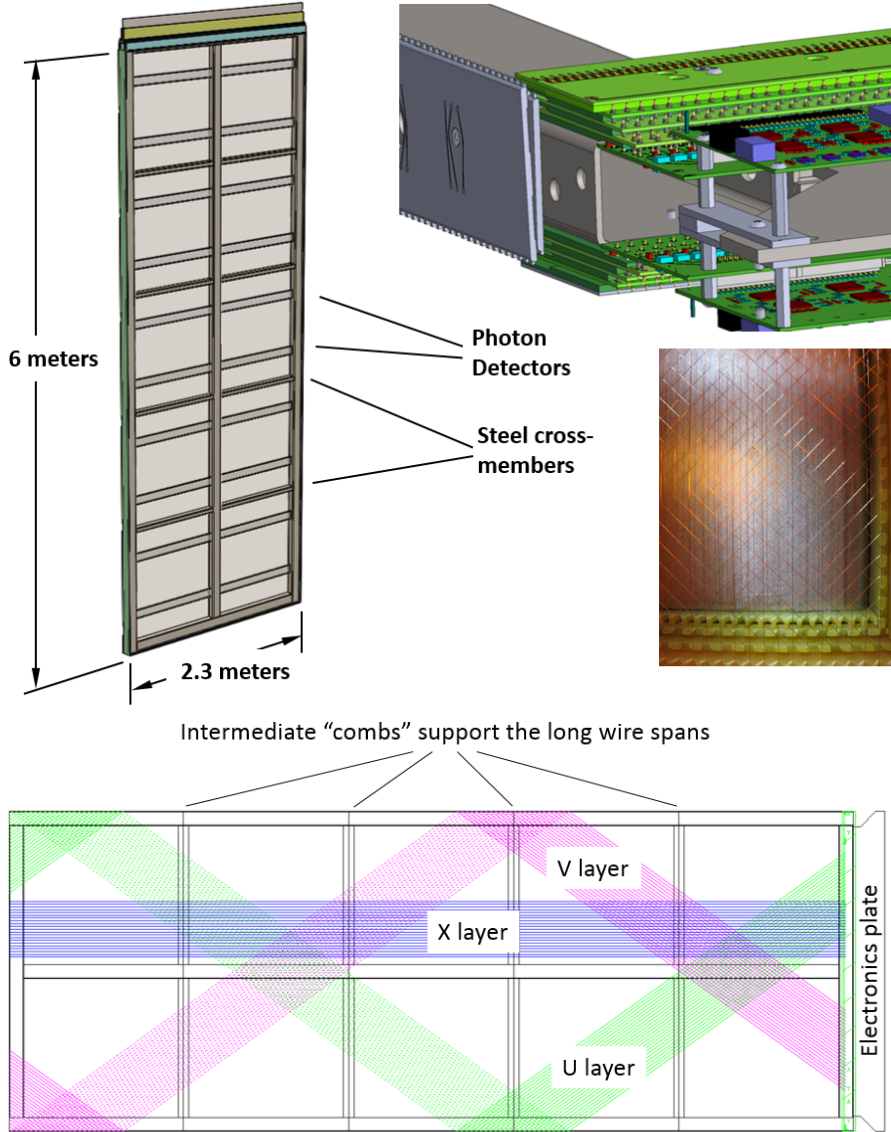


Figure 7: Clockwise from left: A full size APA, an APA corner showing the electronics boards, an APA lower corner photo showing wires and edge boards, and a figure showing the wire orientations and the placement of wire aligning combs.

<sup>459</sup> distorted by the metal frame structure and the wires on the opposite side of the frame. It  
<sup>460</sup> also shields the sensing wires from potential EM interferences from the photon detectors  
<sup>461</sup> (Fig. 3.2.2) mounted within the frame. The mesh should have a wire pitch less than 2  
<sup>462</sup> mm to ensure a uniform electric field while maintaining a high optical transparency.

### <sup>463</sup> 3.2.3 CPA and Field Cage

<sup>464</sup> Each cathode plane (Fig. 9) is constructed from 6 identical CPA (cathode plane assem-  
<sup>465</sup> bly) modules and two sets of end pieces. Each CPA is about half the size of an APA  
<sup>466</sup> ( $2.3\text{m} \times 3.1\text{m}$ ) for ease of assembly and transport. The CPA is made of a stainless-steel  
<sup>467</sup> framework, with 4 pieces of thin FR4 sheets mounted in the openings. A receptacle for

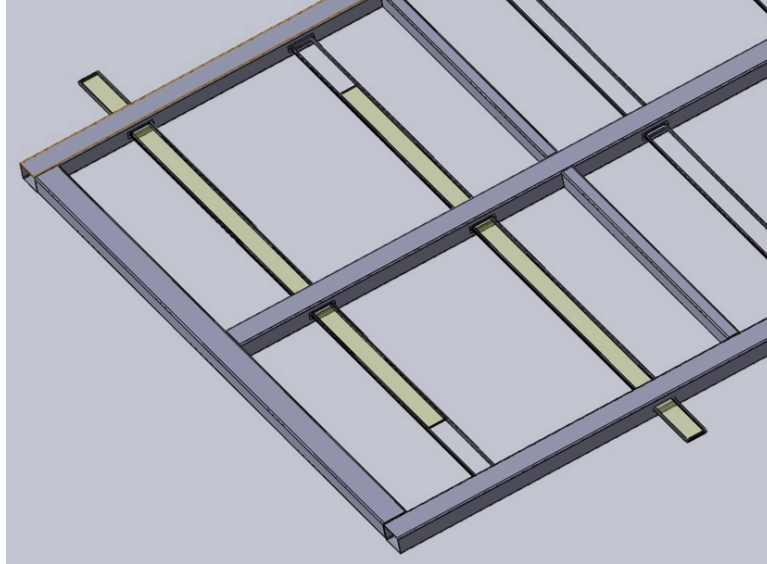


Figure 8: Photon detectors are mounted within the frame, between the wires on the two sets of four wire layers. The APA is built so that the photon detectors can be installed through slots in the side of the APA after the APA wires are installed. The wires that would cross these slots are routed around using copper traces on the edge boards.

468 the HV feedthrough is attached to the upper corner of a cathode plane toward the roof  
 469 entrance side to mate with the HV feedthrough in the cryostat ceiling.

470 The FR4 sheets on the CPAs are treated with layers of high resistive coating on both  
 471 sides. The resistivity of the coating will be chosen such that the surface potential does  
 472 not deviate significantly with the ionization current from the cosmic rays, and forms a  
 473 relatively long time constant to dissipate the stored energy on each sheet in case of a  
 474 high voltage discharge. This long RC time constant will also reduce the peak current  
 475 injected into the front-end electronics in a HV discharge.

476 Due to the relatively high cosmic ray flux in this surface detector, it is preferable to  
 477 prevent the scintillation light emitted by a cosmic ray between the cathode and cryostat  
 478 wall from entering the TPC to reduce false trigger. The opaque cathode surface will  
 479 service this purpose. The high flux of cosmic rays combined with very low drift velocity  
 480 of positive ions in the liquid argon will result in sizable space charge distortions in  
 481 the TPC (docdb #6471). In addition, the positive ions could build up further if the  
 482 ion motion is slowed or stalled by counter flow in the LAr. Preliminary CFD analysis  
 483 (docdb #6140) have shown that solid cathodes in the cryostat result in LAr flow pattern  
 484 that neither causes excess positive ion buildup, nor degrades the LAr purity.

485 To achieve a 500 V/cm drift field over a 2.5 m distance, the bias voltage on the  
 486 cathode plane must reach  $-125$  kV. Two high voltage power supplies ( $150 - 200$  kV) and  
 487 two HV feedthroughs will be needed for the two cathode planes. The HV feedthroughs  
 488 are based on the Icarus design, but modified to further improve the stability at higher  
 489 voltages.

490 Each pair of facing cathode and anode rows forms an electron-drift region. A field  
 491 cage completely surrounds the four open sides of this region to provide the necessary  
 492 boundary conditions to ensure a uniform electric field within, unaffected by the presence

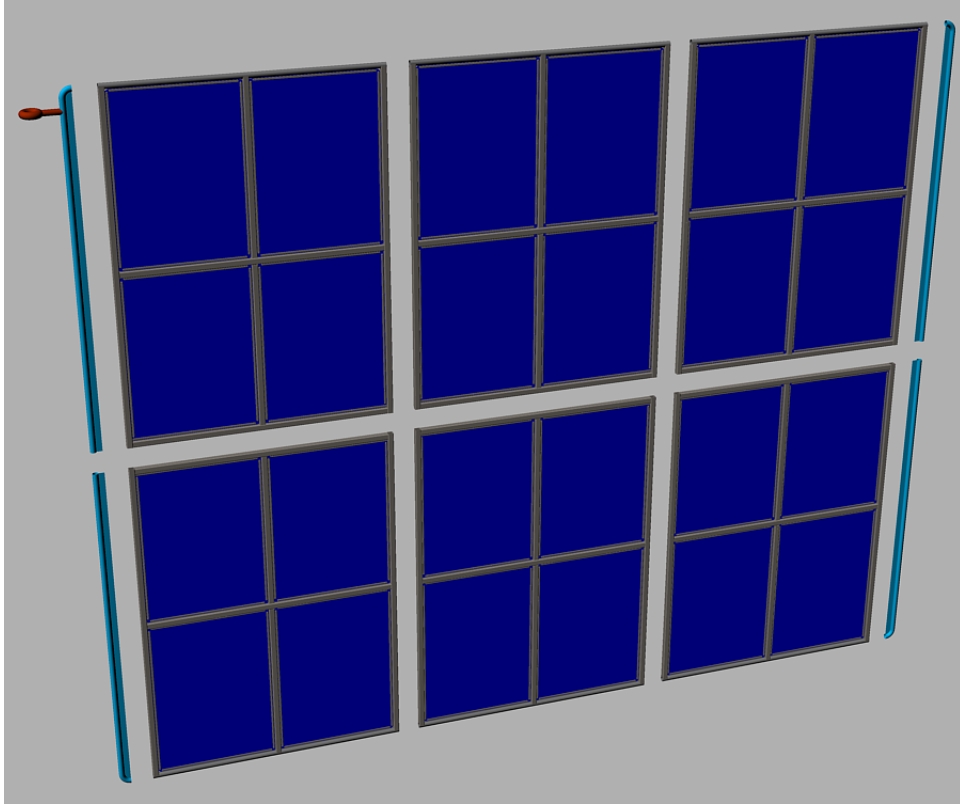


Figure 9: Exploded view of a cathode plane constructed from 6 CPA modules and 4 end pieces. The facing material on the CPA is highly resistive to minimize the peak energy transfer in case of a HV breakdown.

493 of the cryostat walls.

494 The field cages are constructed using copper-clad FR4 sheets reinforced with fiber  
 495 glass I-beams to form panels of  $2.5 \text{ m} \times 2.3 \text{ m}$  in size for the top and bottom modules,  
 496 and  $2.5 \text{ m} \times 2 \text{ m}$  modules for the sides. Parallel copper strips are etched or machined  
 497 on the FR4 sheets. Strips are biased at appropriate voltages through a resistive divider  
 498 network. These strips will create a linear electric-potential gradient in the LAr, ensuring  
 499 a uniform drift field in the TPC's active volume.

500 Since the field cage completely encloses the TPC drift region on four (of six) sides,  
 501 with the remaining two sides blocked by the solid cathodes, the FR4 sheets must be fre-  
 502 quently perforated to allow natural convection of the liquid argon. The “transparency”  
 503 of the perforation will be determined by a detailed LAr computerized fluid dynamic  
 504 (CFD) study.

505 The left of Figure 10 shows a section of the field cage in the 35ton TPC as it was  
 506 being assembled. The 35ton TPC test results will inform us whether we should improve  
 507 upon the current design, or change the design concept all together for this and future  
 508 detectors. The main concern with the current field cage design is that the electric field  
 509 at the edges of the copper strips is still quite high due to the thinness of the copper.  
 510 One possible remedy is to cover the entire surface of the field cage with a high resistive  
 511 coating. The resistivity between strips due to this coating must be kept many orders  
 512 of magnitudes higher than the divider resistance to avoid distortion to the drift field.

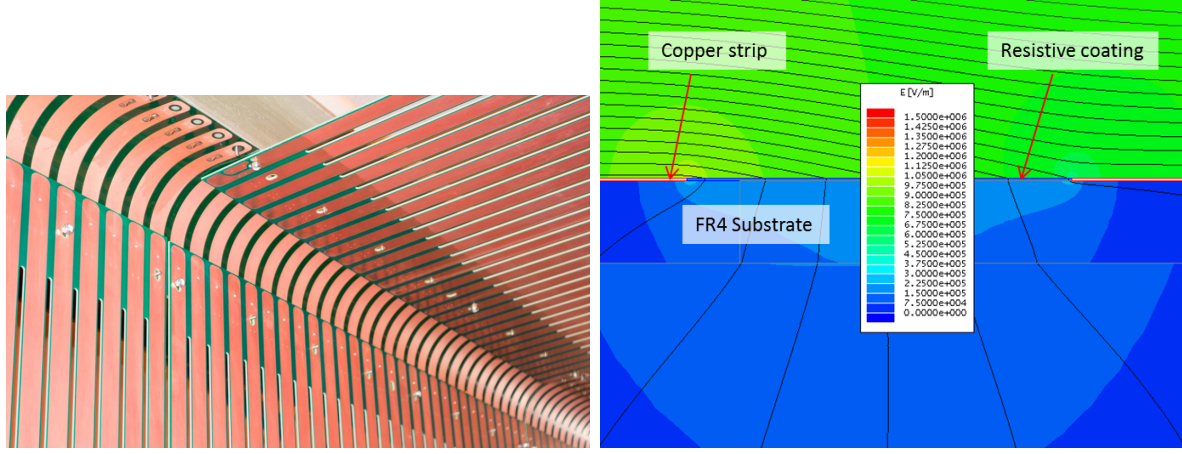


Figure 10: Left: A section of the field cage in the 35ton TPC. Right: Plot of electric field (color contours) and equi-potential contours (black lines) in a small region around the edges of two adjacent field cage strips on a 1.6mm thick FR4 substrate. A layer of resistive coating between the two copper strips nearly eliminated the high electric field regions at the copper edges

513 Figure 10 (Right-Panel) shows an FEA simulation of such a configuration.

514 In the event of HV discharge on the cathode or the field cage, the voltage differential  
 515 between neighboring field cage strips near the discharge electrode will be very high  
 516 for a brief moment. This over voltage condition could cause damage to the field cage  
 517 electrode and the resistors installed between strips. To minimize such disk, varistors or  
 518 gas discharge tubes (GDT) will be installed between the field cage strips in parallel with  
 519 the resistors to prevent excess voltage transient between the electrodes.

520 In order to test the installation concept of the far detector, the top and bottom field  
 521 cage modules will be attached to the mating CPAs through hinges. These combined  
 522 assembly will be installed into the cryostat and the field cage module opens to bridge  
 523 the CPA and the APA both mechanically and electrically.

#### 524 3.2.4 TPC Readout

525 The TPC electronics is designed to operate at liquid argon temperature and is placed as  
 526 close to the sense wires as possible, thus minimizing the capacitance and the preamplifier  
 527 noise. The present design has a maximum wire length of 7.3 m (induction planes) with  
 528 a corresponding capacitance of 164 pF and an expected intrinsic noise of 400 electrons.  
 529 The preamplifiers include shaping circuits, and are implemented in 16 channel front-end  
 530 (FE) ASICs, which couple directly to 16 channel, 12 bit ADC ASICs operating at 2 MS/s,  
 531 which include a 1:8 multiplexing stage. The ADCs are read out by a commercial FPGA,  
 532 which provide an additional factor of 4 in multiplexing. This level of multiplexing is  
 533 low enough for transmitting the entire raw data stream, while also being high enough  
 534 that the number of signal lines is actually smaller than the number of the various power  
 535 and control lines, and therefore easily manageable by a small number of feedthroughs.  
 536 Neither zero suppression nor data compression is implemented at the level of the cold  
 537 readout electronics. Not only does this greatly simplify the cold electronics design, but

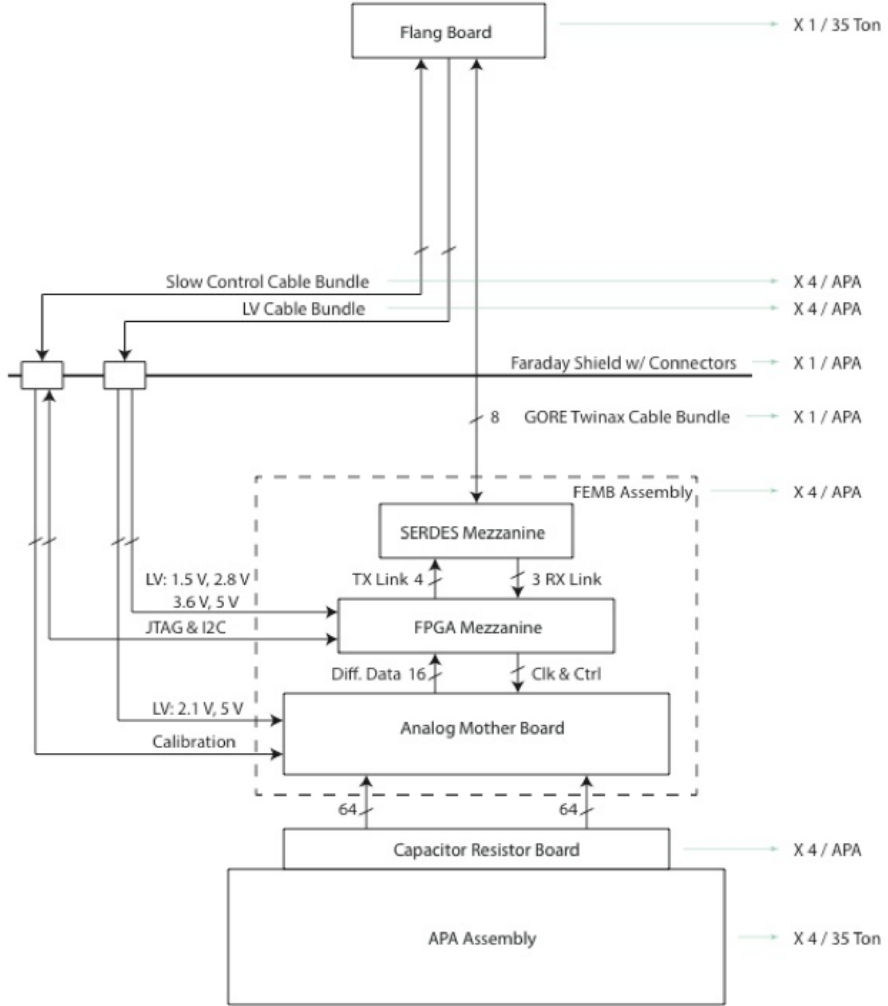


Figure 11: Layout of the TPC cold from end (FE) electronics..

538 it also automatically satisfies the requirement that the system be capable of such raw  
 539 readout, and further eliminates an entire class of failure-modes. The FPGAs transmit  
 540 the data via high-speed (1 Gbps) serial links to the DAQ system. For the final detector  
 541 it is expected that a dedicated digital control and data transmission ASIC (COLDATA)  
 542 will be developed which replaces the commercial FPGA. While the COLDATA is well  
 543 under way, it is not expected to be available in time for the CERN test, which will  
 544 instead make use of the proven FPGA technology. While serious doubts regarding the  
 545 longevity of commercially-available FPGAs at LAr temperatures strongly argues against  
 546 their use in the Far Detector, where reliability over 15-20 years is required, this is not a  
 547 concern for the CERN test, where the proven FPGA lifetime of at least a year is more  
 548 than adequate.

549 The front end electronics is organized as a stack of three boards comprising the Cold  
 550 Mother Board assembly (CMB), which mounts directly on the APA. First is the Analog  
 551 Mother Board, on which are mounted the FE and ADC ASICs. Second and third  
 552 are the FPGA and SERDES Mezzanine Boards, themselves mounted on the Analog

553 Mother Board. Each CMB has eight sets of FE and ADC ASICs and instruments 128  
 554 wires. A Faraday cage (FC) covers the end of the APAs to shield the electronics from  
 555 ambient noise. The FC also serves to prevent any Ar gas-bubbles from LAr boiled by  
 556 the electronics' heat from entering the active TPC volume. Figure 11 shows a schematic  
 557 of the cold electronics.

558 Besides the high-speed signal cable, which is a twin-axial cable bundle manufac-  
 559 tured by GORE, there are cable bundles for low-voltage power, wire-bias voltages, and  
 560 various slow controls and monitoring. The cable bundles will be connected through a  
 561 feedthrough on the roof of the cryostat.

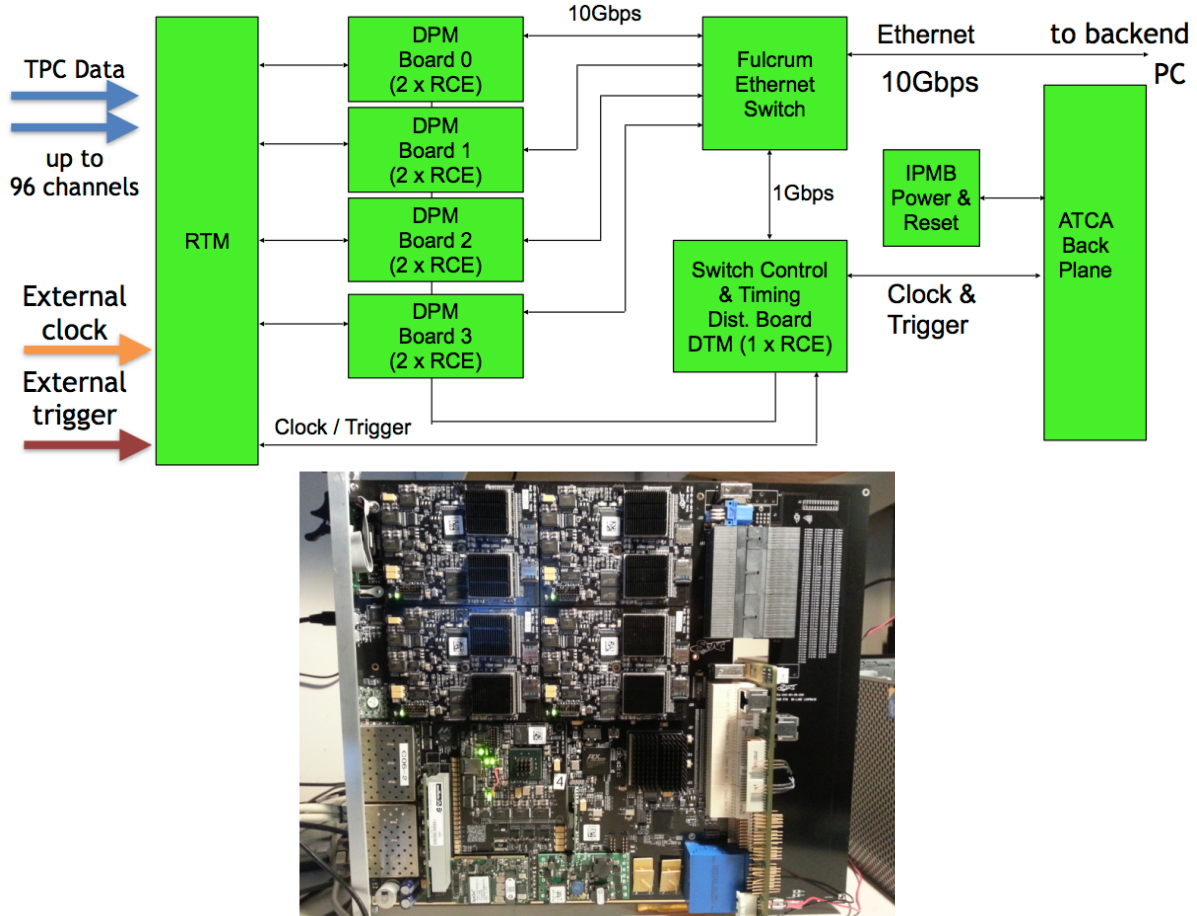


Figure 12: Top: Schematic for the TPC DAQ system. Bottom: The COB (left of the large connectors) and RTM (right).

562 The primary interface between the TPC front-end electronics (FE) and the DAQ sub-  
 563 system consists of an ATCA-based system of RCEs (Reconfigurable Cluster Elements).  
 564 The RCE system receives the serialized raw data for the FE, performs zero-suppression  
 565 on it, and packetizes and transmits the resulting sparsified data to a back-end data farm  
 566 for event building and further processing. Additionally, the RCE system transmits tim-  
 567 ing and control signals to the FE as well as forwarding configuration data to them at  
 568 start-up.

569 The RCE system consists the following components: a commercial ATCA shelf (2-,  
 570 6-, or 14-slot), a Cluster-On-Board (COB) which is the "front board" in ATCA terms,

571 and a Rear-Transition-Module (RTM) which is the "rear board". A schematic of the  
572 system is shown in Figure 12. The COB is a custom board, developed by SLAC, which  
573 holds the processing power of the system. The COB (see Figure 12) consists of 5 bays for  
574 holding daughter boards, an onboard 10-GbE switch, and both 10- and 1-Gb ethernet  
575 connections for communications with the back-end system. Four of the daughter-board  
576 bays are for Data Processing Modules (DPM), each of which can hold up to two RCEs.  
577 The RCE is the core procession unit of the system; it is made up of a modern SoC  
578 (currently, the Xilinx Zynq-7045) with multiple high-speed I/O ports (up to 10-Gbps  
579 each) and external DRAM and flash memory controllers. The other bay on the COB  
580 contains the Data Transmission Module (DTM) which is responsible for distributing  
581 timing and trigger information to and between the DPMs.

582 While the COB hardware is application agnostic, the RTM is application specific.  
583 The RTM provides the mechanical interface between the front-end (or, in our case, the  
584 flange electronics) and the back-end, as well as other external sources such as the timing  
585 or trigger systems. In this case we will use fiber optic connections between the flange  
586 and the TPC DAQ using 8 12-channel (full duplex) CXP connectors on the RTM.

587 With the assumption that each cold FE board multiplexes it's 128 wire channels to 4  
588 outputs at 1-Gbps each, the non-zero suppressed data for 1 APA can be fed into a single  
589 COB (containing 8 RCEs). Each RCE would receive data from 2 FE boards, perform  
590 zero-suppression, and send the result to the back-end.

### 591 3.2.5 Photon Detection System

592 The ELBNF far detector will utilize liquid argon scintillation light to determine the  
593 prompt event time of beam-driven and non-beam events. While the TPC will have far  
594 superior spatial resolution to a photon detection system, the drift time for TPC events  
595 is on the order of milliseconds. The beam clock will give much better timing resolution  
596 than this but a photon detection system can determine the start of an event occurring  
597 in the TPC volume (or entering the volume) to about 6 ns, which will be useful in  
598 determining the  $t_0$  of cosmic ray events, events from radiological decays, and corrections  
599 to energy loss of the drifting electrons.

600 A charged particle passing through liquid argon will produce about 40,000 128 nm  
601 photons per MeV of deposited energy. At higher fields this will be reduced due to  
602 reduced recombination, but at 500 V/cm the yield is still about 20,000 photons per  
603 MeV. Roughly 1/3 of the photons are prompt 2-6 ns and 2/3 are generated with a  
604 delay of 1100-1600 ns. LAr is highly transparent to the 128 nm VUV photons with a  
605 Rayleigh scattering length and absorption length of 95 cm and >200 cm respectively.  
606 The relatively large light yield makes the scintillation process an excellent candidate for  
607 determination of  $t_0$  for non-beam related events. Detection of the scintillation light may  
608 also be helpful in background rejection.

609 Several prototypes of photon detection systems have been developed by the LBNE,  
610 now ELBNF, photon detector group over the past few years. There are currently three  
611 prototypes under consideration for use in the ELBNF far detector, a baseline design  
612 along with two alternate designs. A decision on the design to be deployed in the CERN  
613 test will be made in late 2015. The CERN neutrino platform ELBNF test would provide  
614 the first full scale test of the ELBNF photon detector fully integrated into a full scale

615 TPC anode plane assembly.

616 The present reference design for the photon detection system is based on acrylic bars  
617 that are 200 cm long and 7.63 cm wide, which are coated with a layer of tetraphenyl-  
618 butadiene (TPB). The wavelength shifter converts VUV (128 nm) scintillation photons  
619 striking it to 430 nm photons inside the bar, with an efficiency of 50% of converting  
620 a VUV to an optical photon. A fraction of the wavelength-shifted optical photons are  
621 internally reflected to the bar's end where they are detected by SiPMs whose QE is well  
622 matched to the 430 nm wavelength-shifted photons. All PD prototypes are currently  
623 using SensL MicroFB-6K-35-SMT 6 mm ? 6 mm devices.

624 A full 6 m long APA will be divided into 5 bays with 2 PD modules (paddles)  
625 instrumenting each bay. The paddles will be inserted into the frames after the TPC  
626 wires have been wrapped around the frames allowing final assembly at the CERN test  
627 location. Two alternative designs are also under consideration.

628 One alternate design targeted increasing the geometrical acceptance of the photon de-  
629 tectors by using large acrylic TPB coated plates with imbedded WLS fibers for readout.  
630 In this design the number of required SiPMs and readout channels per unit detector area  
631 covered with photon detection panels would be significantly reduced to keep the overall  
632 cost for the photon detection system at or below the present design while increasing  
633 the geometrical acceptance at the same time. The prototype consists of a TPB-coated  
634 acrylic panel embedded with an S-shaped wavelength shifting (WLS) fiber. The fiber  
635 is read out by two SiPMs, which are coupled to either end of the fiber and serves to  
636 transport the light over long distances with minimal attenuation. The double-ended  
637 fiber readout has the added benefit to provide some position dependence to the light  
638 generation along the panel by comparing relative signal sizes and arrival times in the  
639 two SiPMs.

640 The third design under consideration was motivated by increasing the attenuation  
641 length of the PD paddles and allowing collection of 400 nm photons coming from any-  
642 where in the active volume of the TPC. The fiber-bundle design is based on a thin TPB  
643 coated acrylic radiator located in front of a close packed array of WLS fibers. This  
644 concept is designed so that roughly half of the photons converted in the radiator are  
645 incident on the bundle of fibers, the wavelength shifting fibers are Y11 UV/blue with  
646 a 4% capture probability. The fibers are then read out using SiPMs at one end. The  
647 Y11 Kuraray fibers have mean absorption and emission wavelengths of about 440 nm  
648 and 480 nm respectively. The attenuation length of the Y11 fibers is given to be greater  
649 than 3.5 m at the mean emission wavelength, which will allow production of full-scale  
650 (2 m length) photon detector paddles.

651 The PD system tested at the CERN neutrino platform will be based on technology  
652 selected later this year. The technology selection process will be based on a series of  
653 tests planned for the next 6 months utilizing large research cryostats at Fermilab and  
654 Colorado State University. The primary metric used for comparison between the three  
655 technologies will be photon yield per unit cost. In addition to this metric PD threshold  
656 and reliability will also serve as inputs to the final decision. A technical panel will be  
657 assembled to make an unbiased decision.

658 Once the technology has been chosen the PD group will focus on optimizing the  
659 selected design with the goal of procurement and assembly taking place in late FY 2016  
660 and early FY 2016. The photon detector paddles will then be tested and shipped to

661 CERN in early FY 2017 for installation into the APAs in late FY 2017 in preparation  
662 for installation into the test cryostat and operation in 2018.

### 663 **3.2.6 DAQ, Slow control and monitoring**

664 The DAQ will merge data to form events from the LArTPC, photon detector and beam  
665 detector readouts using the artDAQ data acquisition toolkit using a farm of commercial  
666 computers connected with an Ethernet switch. ArtDAQ is in use on several experiments  
667 at Fermilab. We are using it on the 35t prototype, so we will have considerable experience  
668 by the time of the CERN test.

669 The data collection for the CERN test will operate in a mode similar to that foreseen  
670 for the underground detectors. In order to collect data from non-beam interactions such  
671 as proton decay candidates or atmospheric neutrinos, data will be continuously read in  
672 to the artDAQ data receiver nodes and processed through the artDAQ system in quanta  
673 corresponding to time intervals fixed from the time of the beginning of the run. These  
674 are then transferred through the switch to a set of event building nodes which work in  
675 parallel, each node receiving all the data from all the detectors for the time intervals it  
676 is responsible for processing. There will be 32 parallel incoming data streams from the  
677 LArTPCs and 16 streams from the photon detectors. There will be an additional stream  
678 from the trigger board (the same board as built by Penn for the 35t test will be used)  
679 which will receive input of the spill gate, warning of extraction, and pattern-unit bits  
680 from trigger counters and other beamline instrumentation such as Cerenkov counters  
681 [Which section are these described in?, should we refer to them from here?].

682 Synchronisation across all the input sources is essential in order that artDAQ can  
683 bring together the data from the input streams correctly for processing by the event  
684 building nodes. The data receiver nodes will provide overlap by repeating the data at  
685 the boundaries of the time intervals so that a particle whose data spans two time intervals  
686 can be collected. The time synchronisation is provided to the RTM back-module on the  
687 LArTPC readout crates, to the SSP photon detector readout and to the trigger board  
688 from a GPS based time synchronisation distribution system originally designed for the  
689 NOvA experiment. This system includes functionality to calibrate and correct for the  
690 cable delays, and to send synchronisation control signals to the readout at predetermined  
691 times.

692 The event building nodes will select time regions of interest within the time intervals  
693 they are processing and form these into events to be written to disk. The algorithms  
694 to select the events may be as simple as looking for a trigger bit in the trigger board  
695 data stream, or may involve looking for self-triggered events in the LArTPC data. An  
696 aggregation task, which is part of artDAQ will handle the parallelized event building  
697 processes by merging the output events into a single stream and writing them to disk. To  
698 avoid oversized output data files, when a predetrmined file size is reached, the aggregator  
699 will switch to writing to a new file. The collaboraion requests to CERN, data links of  
700 sufficient bandwidth to transfer these files from the CENF to the CERN data center,  
701 and from there to locations worldwide for analysis.

702 Improved versions of the software systems which are being prototyped at the 35t test  
703 will available for the CERN test including (a) Run control which controls and monitors  
704 the DAQ processes and allows run starts and stops to be performed by the operator

705 (b) online monitoring (c) slow control of voltages and temperatures being used by the  
706 electronics (this may not be comprehensive by the time of the CERN prototype, but we  
707 plan on prototyping the readout of some of the quantities). The trigger board includes  
708 facilities for generating calibration pulses and for identifying the event times of the  
709 calibration events.

710 **3.2.7 Installation**

711 The interior of the cryostat will be prepared prior to the installation of the TPC. A series  
712 of support rails will be suspended below the top surface of the cryostat membrane. These  
713 will be structurally supported by a truss structure above the cryostat. These supports  
714 will pass through the top of the cryostat. They need to be designed to minimize the heat  
715 gain into the cryogenic volume. For the CPAs, the rails need to be electrically isolated  
716 due to high voltage concerns. To preserve the ability to reverse the order of the TPC  
717 components, all of the support rails will be designed to the same set of requirements  
718 regarding loads and attachment points.

719 There will be a series of feed thru flanges located along each of the support rails.  
720 These will be cryogenic flanges where the services for the TPC components can pass  
721 through the top of the cryostat. It is foreseen that each CPA will require one feed thru  
722 for the high voltage probe to bring in the drift voltage. The drift voltage is 500 V/cm.  
723 For a drift distance of 2.5 m, the probe voltage will be 125 kV. There will be one service  
724 feed thru for each of the APAs. These feed thrus will include high speed data, bias  
725 voltages for the wire planes, control and power for the cold electronics.

726 The main TPC components will be installed through a large hatch in the top of the cryostat.  
727 This is similar to the installation method intended for the detector at the far  
728 site. This hatch will have an aperture approximately 2.0 m wide and 3.5 m long. Each  
729 APA and CPA panel will be carefully tested after transport into the clean area and  
730 before installation into one of the cryostats. Immediately after a panel is installed it will  
731 be rechecked. The serial installation of the APAs along the rails means that removing  
732 and replacing one of the early panels in the row after others are installed would be very  
733 costly in effort and time. Therefore, to minimize the risk of damage, as much work  
734 around already installed panels as possible will be completed before proceeding with  
735 further panels. The installation sequence is planned to proceed as follows:

- 736 1. Install the monorail or crane in the staging area outside the cryostat, near the  
737 equipment hatch.
- 738 2. Install the relay racks on the top of the cryostat and load with the DAQ and power  
739 supply crates.
- 740 3. Dress cables from the DAQ on the top of the cryostat to remote racks.
- 741 4. Construct the clean-room enclosure outside the cryostat hatch.
- 742 5. Install the raised-panel floor inside the cryostat.
- 743 6. Insert and assemble the stair tower and scaffolding in the cryostat.
- 744 7. Install the staging platform at the hatch entrance into the cryostat.

- 745        8. Install protection on (or remove) existing cryogenics instrumentation in the cryo-  
746        stat.
- 747        9. Install the cryostat feedthroughs and dress cables inside the cryostat along the  
748        support beams.
- 749        10. Install TPC panels:
- 750              (a) Install both pairs of CPA panels. These will be installed from the floor of the  
751        cryostat. Access to the top edge will be required by scaffolding.
- 752              (b) Install and connect HV probe for each of the CPAs.
- 753              (c) Perform electrical tests on the connectivity of the probe to the CPAs.
- 754              (d) Install first end wall of vertical field cage at the non-access end of the cryostat.  
755        These will be installed from the floor of the cryostat. Scaffolding will be  
756        needed to install the supporting structure and then attach the panels to the  
757        structure.
- 758              (e) Test the inner connections of the field cage panels.
- 759              (f) Install the first APA and connect to the far end field cage support.
- 760              (g) Connect power and signal cables. This will require scaffolding to access the  
761        top edge of the APA.
- 762              (h) Test each APA wire for expected electronics noise. Spot-check electronics  
763        noise while cryogenics equipment is operating.
- 764              (i) Install the upper field cage panels for the first APA between the APA and  
765        CPAs. This will require scaffolding to access the upper edge of the APA, CPA  
766        and field cage structure.
- 767              (j) Perform electrical tests on upper field cage panels.
- 768              (k) Repeat steps (f) through (j) for the next two APAs.
- 769              (l) Install the lower field cage panels between the APAs and CPAs. Start at the  
770        far end away from the access hatch and work towards the hatch.
- 771              (m) Perform electrical test on lower field cage panels and the entire loop around  
772        the TPC.
- 773              (n) Remove temporary floor sections as the TPC installation progresses.
- 774              (o) Install sections of argon-distribution piping as the TPC installation pro-  
775        gresses.
- 776              (p) Install the final end wall of vertical field cage at the access end of the cryostat.  
777        These will be installed from the floor of the cryostat. Scaffolding will be  
778        needed to install the supporting structure and then attach the panels to the  
779        structure.
- 780        11. Remove movable scaffold and stair towers.
- 781        12. Temporarily seal the cryostat and test all channels for expected electronics noise.

- 782     13. Seal the access hatch.
- 783     14. Perform final test of all channels for expected electronics noise.

784     In general, APA panels will be installed in order starting with the panel furthest  
785     from the hatch side of the cryostat and progressing back towards the hatch. The upper  
786     field cage will be installed in stages as the installation of APA and CPAs progresses.  
787     After the APAs are attached to the support rods the electrical connections will be made  
788     to electrical cables that were already dressed to the support beams and electrical testing  
789     will begin. Periodic electrical testing will continue to assure that nothing gets damaged  
790     during the additional work around the installed APAs.

791     The TPC installation will be performed in three stages, each in a separate location;  
792     the locations, or zones. First, in the clean room vestibule, a crew will move the APA and  
793     CPA panels from storage racks, rotate to the vertical position and move them into the  
794     cryostat. Secondly, in the panel-staging area immediately below the equipment hatch  
795     of the cryostat, a second crew will transfer the panels from the crane to the staging  
796     platform, where the crew inside the cryostat will connect the to the rails within the  
797     cryostat. A third crew will reposition the movable scaffolding and use the scaffold to  
798     make the mechanical and electrical connections at the top for each APA and CPA as  
799     they are moved into position.

800     The requirements for alignment and survey of the TPC are under development.  
801     Since there are many cosmic rays in the surface detector and beam events, significant  
802     corrections can be made for any misalignment of the TPC. The current plan includes  
803     using a laser guide or optical transit and the adjustment features of the support rods  
804     for the TPC to align the top edges of the APAs in the TPC to be straight, level and  
805     parallel within a few mm. The alignment of the TPC in other dimensions will depend  
806     on the internal connecting features of the TPC. The timing of the survey will depend  
807     on understanding when during the installation process the hanging TPC elements are  
808     in a dimensionally stable state. The required accuracy of the survey is not expected to  
809     be more precise than a few mm.

## 810    **4 Cryostat and cryogenics system [~5 pages; David/Barry/Jack]**

### 811    **4.1 Cryostat**

812     The Single Phase TPC test at CERN will use a membrane tank technology to contain  
813     725 tons of LAr, equivalent to about  $520m^3$ . The design is based on a scaled up version of  
814     the LBNE 35-ton Prototype [4] and the Fermilab Short-Baseline Near Detector [5]. The  
815     cryostat will use a steel outer supporting structure with a metal liner inside to isolate  
816     the insulation volume, similar to the one of the dual phase detector prototype WA105  
817      $1 \times 1 \times 3$  and to the Fermilab Short-Baseline Near Detector. The support structure  
818     will rest on I-beams to allow for air circulation underneath in order to maintain the  
819     temperature within the allowable limits. This section describes the proposed design,  
820     whose scope encompasses the following components:

- 821       • steel outer supporting structure,

- 822     • main body of the membrane cryostat (sides and floor),  
823     • top cap of the membrane cryostat.

824     A membrane cryostat design commonly used for liquefied natural gas (LNG) storage  
825     and transportation will be used. In this vessel a stainless steel membrane contains  
826     the liquid cryogen. The pressure loading of the liquid cryogen is transmitted through  
827     rigid foam insulation to the surrounding outer support structure, which provides external  
828     support. The membrane is corrugated to provide strain relief resulting from temperature  
829     related expansion and contraction. The vessel is completed with a top cap that uses the  
830     same technology.

831     Two membrane cryostat vendors are known: GTT (Gaztransport & Technigaz) from  
832     France and IHI (Ishikawajima-Harima Heavy Industries) from Japan. Each one is tech-  
833     nically capable of delivering a membrane cryostat that meets the design requirements  
834     for this detector. To provide clarity, only one vendor is represented in this document,  
835     GTT; this is for informational purposes only. Figure 1 shows a 3D model of the GTT  
836     membrane and insulation design.

837     The conceptual proposed design for the Single Phase Test at CERN cryostat is a  
838     rectangular vessel measuring 9.5 m in length (parallel to the beam direction), 7.3 m in  
839     width, and 8.40 m in height; containing a total mass of 725 tons of liquid argon. Figure 15  
840     shows side and end views of the cryostat respectively. Figure 3 shows a 3D view. To  
841     minimize the contamination from warm surfaces, during operation the temperature of all  
842     surfaces in the ullage shall be lower than 100 K. The top plate will contain two hatches,  
843     one to install the TPCs and the other to access the tank; it will also contain a manhole  
844     to enter the tank after closing the hatches, and several penetrations for the cryogenic  
845     system and the detector.

#### 846     **Design Parameters**

847     This design includes technical solutions that may be of interested for the future needs  
848     of the Long Baseline Neutrino program. For example the use of a cold ullage (<100 K)  
849     to lower the impurities in the gas region, and of a LAr pump outside the cryostat to  
850     minimize the effect of noise, vibration and microphonics to the TPC inside the liquid  
851     argon volume.

852     The design parameters for the TPC Test at CERN cryostat are listed in Table 6.

#### 853     **Insulation system and secondary membrane**

854     The membrane cryostat requires insulation applied to all internal surfaces of the  
855     outer support structure and roof in order to control the heat ingress and hence required  
856     refrigeration heat load. To avoid bubbling of the liquid Argon inside the tank, the  
857     maximum static heat leak is  $10W/m^2$  for the floor and the sides and  $15W/m^2$  for the  
858     roof, higher to account for the penetrations that increase the heat budget. Preliminary  
859     calculations show that these values it can be obtained using 0.9 m thick insulation  
860     panels of polyurethane foam. Given an average thermal conductivity coefficient for the  
861     insulation material of  $0.0283 \text{ W}/(\text{m}\cdot\text{K})$ , the heat input from the surrounding steel is  
862     expected to be about 3.4 kW total. It assumes that the hatches are foam insulated as  
863     well. This is shown in Table 7.

864     The insulation material is a solid reinforced polyurethane foam manufactured as  
865     composite panels. The panels get laid out in a grid with 3 cm gaps between them  
866     (that will be filled with fiberglass) and fixed onto anchor bolts anchored to the support

# GST® Containment System

## AS A PRIMARY BARRIER :

### a flexible (1.2mm) stainless steel membrane



The double network of corrugations absorbs the thermal contractions due to the very low temperature of the LNG.

## Insulating panel

The thickness of the panels can be adjusted to provide a large range of boil-off rates according to the operator's requirements (typically 0.05% per day).

### Plywood

### Reinforced polyurethane foam

## AS A SECONDARY BARRIER :

### a composite laminated material

This consists of a thin sheet of aluminium between two layers of glass cloth and resin.

In the event of a failure of the primary membrane, it prevents the build-up of stress concentrations on concrete corner and ensures the liquid tightness of the concrete wall.

### Reinforced polyurethane foam

### Plywood

### Mastic

## Post-tensionned concrete covered by a moisture barrier

The outer concrete container provides the *structural resistance* to internal (LNG hydrostatic & dynamic pressure, and vapour gas pressure) and external (wind, snow, ice) loads.

A moisture barrier, applied on its inner side, prevents moisture from entering the tank.

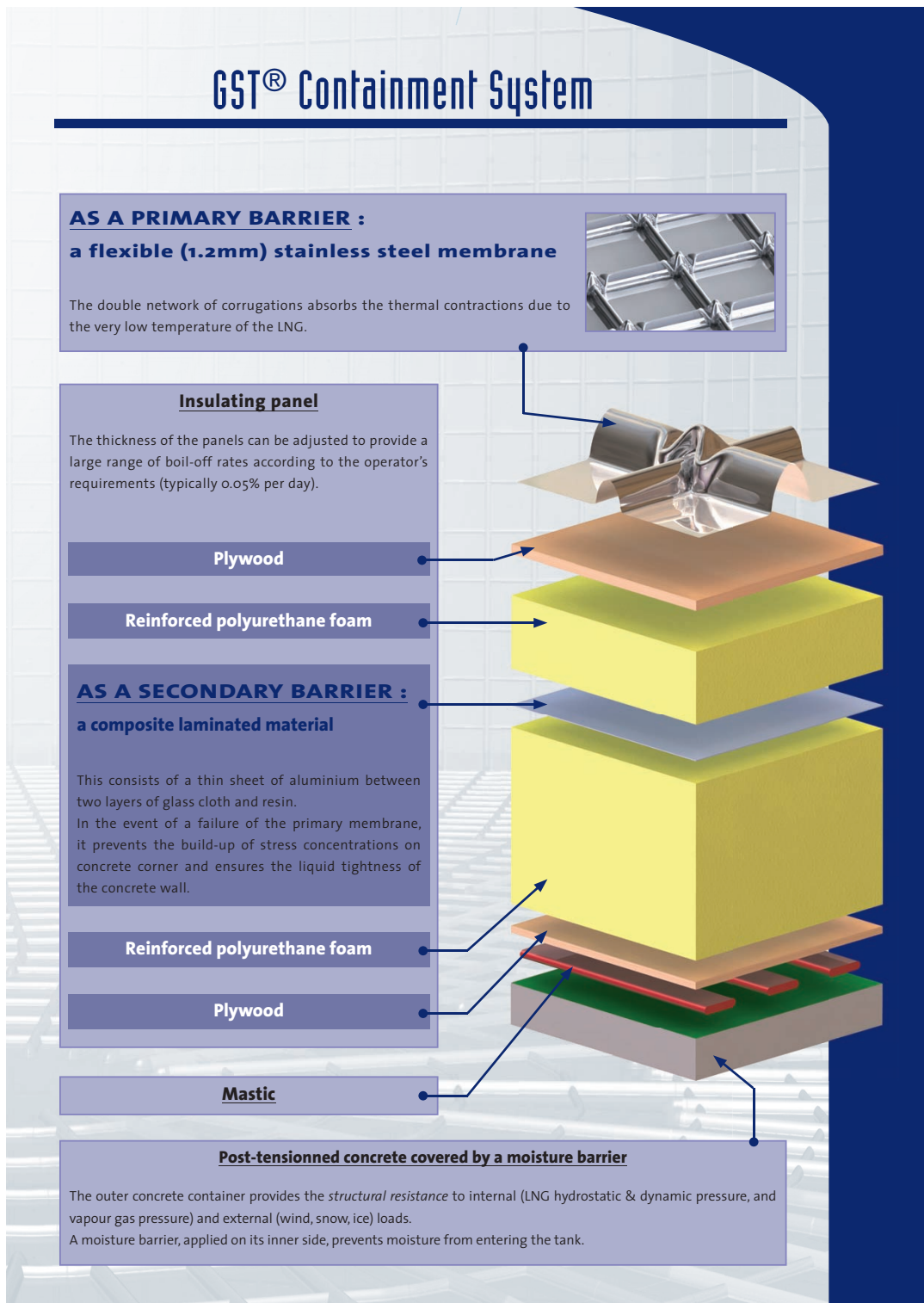


Figure 13: Exploded view of the membrane cryostat technology

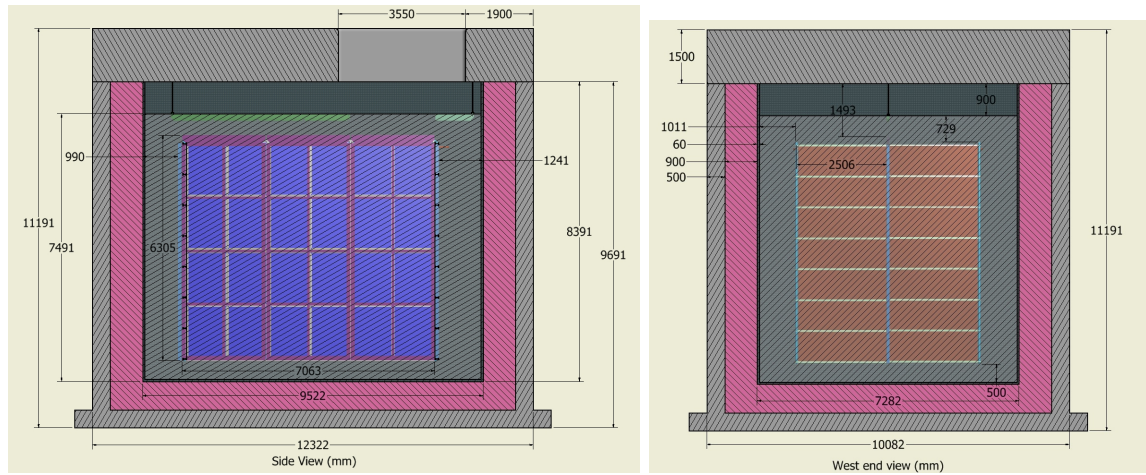


Figure 14: Side (left) and end (right) views of cryostat

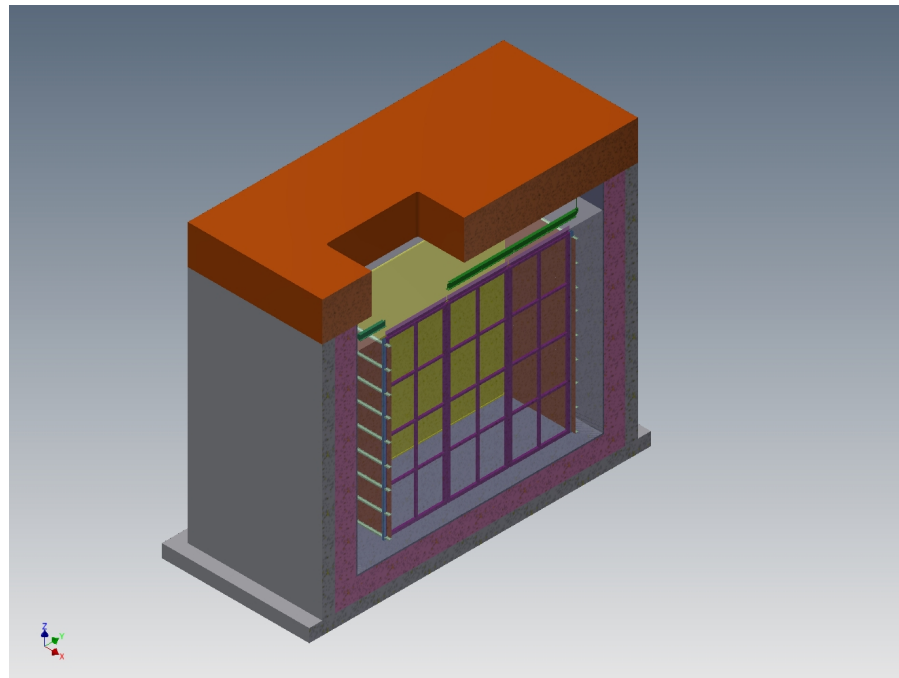


Figure 15: Isometric view of the membrane cryostat

Table 6: Design requirements for the membrane cryostat

<b>Design Parameter</b>	<b>Value</b>
Type of structure	Membrane cryostat
Membrane material	SS 304/304L, 316/316L or equivalent.
Fluid	Liquid argon (LAr)
Other materials upon approval.	
Outside reinforcement (support structure)	Steel enclosure with metal liner to isolate the outside from the insulation space, standing on legs to allow for air circulation underneath.
Total cryostat volume	583 m3
Total LAr volume	520 m3
LAr total mass	725,000 kg
Minimum inner dimensions (flat plate to flat plate).	7.3 m (W) x 9.5 m (L) x 8.4 m (H)
Depth of LAr	7.5 m (0.9 m ullage, same as LBNF)
Primary membrane	1.2 mm thick SS 304L corrugated stainless steel
Secondary barrier system	GTT design; 0.07 mm thick aluminum between fiberglass cloth. Overall thickness 1 mm located between insulation layers.
Insulation	Polyurethane foam (0.9 m thick from preliminary calculations)
Maximum static heat leak	10 W/m2
LAr temperature	88 +/- 1K
Operating gas pressure	Positive pressure. Nominally 70 mbarg (~1 psig)
Vacuum	No vacuum
Design pressure	350 mbarg (~5 psig) + LAr head (1,025 mbarg)
Design temperature	77 K (liquid nitrogen temperature for flexibility)
Temperature of all surfaces in the ullage during operation	<100 K
Leak tightness	$1e - 6$ mbar*l/sec
Maximum noise/vibration/microphonics inside the cryostat	LAr pump outside the cryostat
Beam window	Precise location TBD. Figure 15 shows the location where the beam enters the cryostat.
Accessibility after operations	Capability to empty the cryostat in 30 days and access it in 60 days after the end of operations.
Lifetime / Thermal cycles	Consistent with liquid argon program. TBD.

867 structure. The composite panels contain the two layers of insulation with the secondary  
868 barrier in between. After positioning adjacent composite panels and filling the 3-cm  
869 gap, the secondary membrane is spliced together by epoxying an additional overlapping  
870 layer of secondary membrane over the joint. All seams are covered so that the secondary  
871 membrane is a continuous liner.

872 In the current GTT design, the secondary membrane is comprised of a thin aluminum  
873 sheet and fiberglass cloth. The fiberglass-aluminum-fiberglass composite is very durable  
874 and flexible with an overall thickness of about 1 mm. The secondary membrane is placed  
875 within the insulation space. It surrounds the bottom and sides. In the unlikely event of  
876 an internal leak from the primary membrane of the cryostat into the insulation space, it  
877 will prevent the liquid cryogen from migrating all the way through to the steel support  
878 structure where it would degrade the insulation thermal performance and could possibly  
879 cause excessive thermal stress in the support structure. The liquid cryogen, in case of  
880 leakage through the inner (primary) membrane will escape to the insulation volume,  
881 which is purged with GAr at the rate of one volume exchange per day.

Table 7: Heat load calculation for the membrane cryostat (insulation thickness = 0.9 m). (note to self: has right values)

Element	Area ( $m^2$ )	K (W/mK)	$\Delta T$ (K)	Heat Input (W)
Base	83	0.0283	205	550
End walls	190	0.0283	205	1,247
Side walls	149	0.0283	205	983
Roof	83	0.0283	205	550
Total				3,330

## 882 Cryostat Configuration

883 With the intent to minimize the contamination in the gas region, the ullage will be  
884 kept cold (<100 K). It has been observed in the Materials Test Stand (MTS) and the  
885 Liquid Argon Purity Demonstrator (LAPD) at Fermilab that the outgassing is signifi-  
886 cantly reduced below 100 K [add reference]. A possible way to achieve this requirement  
887 is to spray a mist of clean liquid and gaseous argon to the metal surfaces in the ullage  
888 and keep them cold, similar to the strategy that was developed for the cool down of the  
889 LBNE 35 Ton prototype.

## 890 Outer Support Structure

891 The proposed design is a steel support structure with a metal liner on the inside  
892 to isolate the insulation region and keep the moisture out. This choice allows natural  
893 and forced ventilation to maintain the temperature of the steel within its limit, without  
894 the need of heating elements and temperature sensors. It reduces the time needed for  
895 the construction: the structure will be prefabricated in pieces of dimensions appropriate  
896 for transportation, shipped to the destination and only assembled in place. Fabrication  
897 will take place at the vendor's facility for the most part. This shortens the construction  
898 of the outer structure on the detector site, leaving more time for completion of the  
899 building infrastructure. If properly designed, a steel structure may allow the cryostat to  
900 be moved, should that be desired in the future.

901      **Main body of the membrane cryostat**

902      The sides and bottom of the vessel constitute the main body of the membrane cryo-  
903      stat. They consist of several layers. From the inside to the outside the layers are stainless  
904      steel primary membrane, insulation, thin aluminum secondary membrane, more insula-  
905      tion, and steel outer support structure with metal panels acting as vapor barrier. The  
906      secondary membrane contains the LAr in case of any primary membrane leaks and  
907      the vapor barrier prevents water ingress into the insulation. The main body does not  
908      have side openings for construction. The access is only from the top. There is a side  
909      penetration for the liquid argon pump for the purification of the cryogen.

910      **Top cap**

911      Several steel reinforced plates welded together constitute the top cap. The stainless  
912      steel primary membrane, intermediate insulation layers and vapor barrier continue across  
913      the top of the detector, providing a leak tight seal. The secondary barrier is not used  
914      nor required at the top. The cryostat roof is a removable steel truss structure that also  
915      supports the detector. Stiffened steel plates are welded to the underside of the truss to  
916      form a flat vapor barrier surface onto which the roof insulation attaches directly. The  
917      penetrations will be clustered in the back region. The top cap will have a large opening  
918      for TPC installation, a secondary smaller opening for personnel access and a manhole  
919      to enter the tank after the hatches have been closed.

920      The truss structure rests on the top of the supporting structure where a positive  
921      structural connection between the two is made to resist the upward force caused by the  
922      slightly pressurized argon in the ullage space. The hydrostatic load of the LAr in the  
923      cryostat is carried by the floor and the sidewalls. Everything else within the cryostat  
924      (TPC planes, electronics, sensors, cryogenic and gas plumbing connections) is supported  
925      by the steel plates under the truss structure. All piping and electrical penetration into  
926      the interior of the cryostat are made through this top plate, primarily in the region of  
927      the penetrations to minimize the potential for leaks. Studs are welded to the underside  
928      of the top plate to bolt the insulation panels. Insulation plugs are inserted into the  
929      bolt-access holes after panels are mounted. The primary membrane panels are first  
930      tack-welded then fully welded to complete the inner cryostat volume.

931      Table 8 presents the list of the design parameters for the top of the cryostat.

932      **Cryostat grounding and isolation requirements**

933      The cryostat has to be grounded and electrically isolated from the building. This  
934      section presents the list of the current grounding and isolation requirements for the  
935      cryostat. Figure 16 shows the layout of the top plate grounding.

936      **Isolation**

- 937      1. The cryostat membrane and any supporting structure, whether it is a steel struc-  
938      ture or a concrete and rebar pour, shall be isolated from any building metal or  
939      building rebar with a DC impedance greater than 300 kΩ.
- 940      2. All conductive piping penetrations through the cryostat shall have dielectric breaks  
941      prior to entering the cryostat and the top plate.

942      **Grounding**

- 943      1. The cryostat, or “detector” ground, shall be separated from the “building” ground.

Table 8: Design parameters for the top of the cryostat

<b>Design Parameter</b>	<b>Value</b>
Configuration	Removable metal plate reinforced with trusses/I-beams anchored to the membrane cryostat support structure. Contains multiple penetrations of various sizes and a man-hole. Number, location and size of the penetrations TBD. Provisions shall be made to allow for removal and re-welding six (6) times.
Plate/Trusses non-wet material	Steel if room temperature. SS 304/304 or equivalent if at cryogenic temperature
Wet material	SS 304/304L, 316/316L or equivalent. Other materials upon approval.
Fluid	Liquid argon (LAr)
Design pressure	350 mbarg ( 5 psig)
Design temperature	77 K (liquid nitrogen temperature for flexibility)
Inner dimensions	To match the cryostat
Maximum allowable roof deflection	0.028 m (span/360 from LBNF)
Maximum static heat leak	<15 W/m <sup>2</sup>
Temperatures of all surfaces in the ullage during operation	<100 K
Additional design loads	<ul style="list-style-type: none"> <li>- Top self-weight</li> <li>- TPC ( 3,000 kg on each anchor)</li> <li>- TPC anchors (TBD)</li> <li>- Live load (488 kg/m<sup>2</sup>)</li> <li>- Electronics racks (400 kg in the vicinity of the feed through)</li> <li>- Services (150 kg on every feed through)</li> </ul>
TPC anchors	Capacity: 3,000 kg each anchor. Number and location TBD. Minimum 6.
Hatch opening for TPC installation	3,550 m x 2,000 m (location TBD)
Grounding plate	1.6 mm thick copper sheet brazed to the bottom of the top plate
Lifting fixtures	Appropriate for positioning the top at the different parts that constitute it.
Cold penetrations	Location and design TBD.
Lifetime / Thermal cycles	Consistent with the liquid argon program TBD.

- 944     2. A safety ground network consisting of saturated inductors shall be used between  
945       detector ground and building ground.
- 946     3. Parameters TBD.

947     **Top plate grounding**

- 948     1. If the cryostat is contained within a concrete pour, the top plate shall be electrically  
949       connected to any rebar used in that pour, and the rebar shall be conductively tied  
950       at regular intervals. Parameters TBD.
- 951     2. The top grounding plate shall be electrically connected to the cryostat membrane  
952       by means of copper braid connections.
- 953       (a) Each connection shall be at least 1.6 mm thick and 63.5 mm wide.
- 954       (b) The length of each connection is required to be as short as possible.
- 955       (c) The distance between one connection and the next one shall be no more than  
956        1.25 m.
- 957       (d) The layout can follow the profile of several pieces of insulation, but it shall  
958        be continuous.
- 959       (e) The DC impedance of the membrane to the top plate shall be less than 1  
960        ohm.

961     **Leak prevention**

962     The primary membrane will be subjected to several leak tests and weld remediation,  
963     as necessary. All (100%) of the welds will be tested by an Ammonia colorimetric leak  
964     test (ASTM E1066-95) in which welds are painted with a reactive yellow paint before  
965     injecting a Nitrogen-Ammonia mixture into the insulation space of the tank. Wherever  
966     the paint turns purple or blue, a leak is present. The developer is removed, the weld  
967     fixed and the test is performed another time. Any and all leaks will be repaired. The  
968     test lasts a minimum of 20 hours and is sensitive enough to detect defects down to  
969     0.003 mm in size and to a  $10^{-7} \text{ std } - \text{cm}^3/\text{s}$  leak rate (equivalent leak rate at standard  
970     pressure and temperature, 1 bar and 273 K). To prevent infiltration of water vapor  
971     or oxygen through microscopic membrane leaks (below detection level) the insulation  
972     spaces will be continuously purged with gaseous argon to provide one volume exchange  
973     per day. The insulation space will be maintained at 70 mbar, slightly above atmospheric  
974     pressure. This space will be monitored for changes that might indicate a leak from the  
975     primary membrane. Pressure control devices and safety relief valves will be installed on  
976     the insulation space to ensure that the pressure does not exceed the operating pressure  
977     inside the tank. The purge gas will be recirculated by a blower, purified, and reused as  
978     purge gas. The purge system is not safety- critical; an outage of the purge blower would  
979     have negligible impact on LAr purity.

980     **4.2 Cryostat size from TPC dimensions (Move to begining of  
981       sec 4 per DM)**

982     The minimum internal size of the cryostat is determined from size of the TPC. At the  
983     bottom of the cryostat there needs to be a minimum of 0.3 m between the frame of the

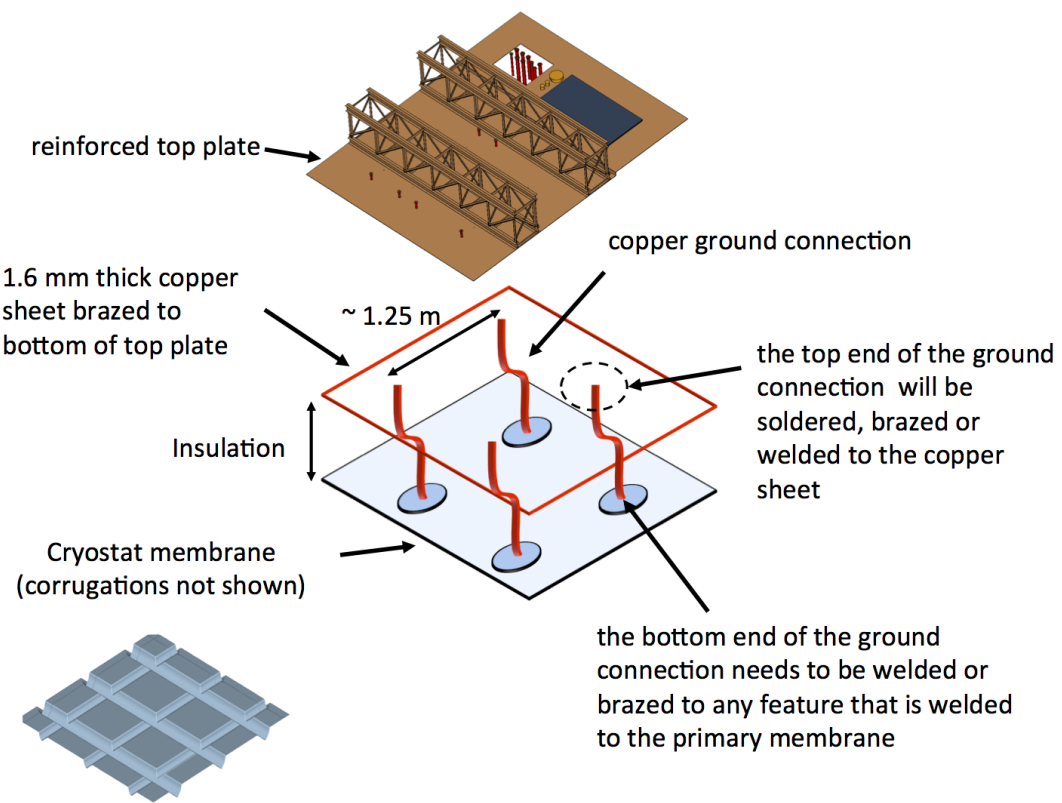


Figure 16: Top plate grounding layout

984 CPA and closest point on the SS membrane. This is to prevent high voltage discharge  
985 between the CPA and the electrically grounded membrane. It is foreseen that there  
986 would be some cryogenic piping and instrumentation under the TPC. There is a height  
987 allowance of 0.1 m for this. There will be access and egress space around the outside of  
988 the TPC and the membrane walls. On three sides, 1.0 m of space is reserved for this.  
989 The final side of the TPC will have piping and instrumentation for the cryogenic system.  
990 There will be 1.3 m of space reserved for this.

991 The support system for the TPC will be located at the top between the underside  
992 of the cryostat roof and the top of the TPC. The plan is to model this space similar to  
993 what is planned for the far site TPC. There will be 0.9 m of ullage space. In order to  
994 prevent high voltage discharge, the upper most part of the CPA needs to be submerged a  
995 minimum of 0.3 m below the liquid Argon surface. The top of the TPC will be separated  
996 from the membrane by a minimum of 1.2 m.

997 Adding all of these to the size of the TPC yields the minimum inner dimensions of  
998 the cryostat. A minimally sized cryostat would be 9.5 m long, 7.3 m wide and 8.4 m  
999 high. This assumes the TPC will be positioned inside the cryostat with the CPAs and  
1000 end field cages parallel to the walls of the cryostat. Also there is no space allotted for  
1001 a beam window to enter the cryostat. Clearance would need to be added if it violates  
1002 any of the current boundaries listed above. These dimensions also preserve the ability  
1003 to reverse the order of the APAs and CPAs inside the TPC. The current plan is to have  
1004 the APAs located in the center of the cryostat with a CPA on each side. Reversing this  
1005 to have the CPA in the center and APAs on each side may be required to achieve some  
1006 of the proposed physics. The orientation of the TPC components will be finalized after  
1007 various scenarios have been sufficiently simulated.

### 1008 4.3 Cryogenic System

1009 Figure 17 outlines the basic scheme of the LN2 supply system, which was proposed  
1010 by CERN for the Short Baseline Program and found to be an appropriate solution for  
1011 this detector as well. The experiment will rely on LN2 tankers for regular deliveries to a  
1012 local dewar storage, which will be sized to provide several days of cooling capacity in the  
1013 event of a delivery interruption. From the dewar storage the LN2 is then transferred to  
1014 a distribution facility located in the experimental hall. It includes a small buffer volume  
1015 and an LN2 pumping station that transfers the LN2 to the argon condenser and other  
1016 services as needed. The low estimated heat leak of the vessel ( $\sim 3.4$  kW) and the location  
1017 inside an above ground building allow for use of an open loop system typical of other  
1018 installations operated at Fermilab (LAPD, LBNE 35 ton prototype, MicroBooNE) and  
1019 at CERN (???). Main goal of the LN2 system is to provide cooling power for the argon  
1020 condenser, the initial cool down of the vessel and the detector, and all other services as  
1021 needed.

1022 Table 9 presents the list of requirements for the cryogenic system for the Single Phase  
1023 TPC test at CERN detector.

1024 Figure 18 shows a schematic diagram of the proposed liquid argon system. It is based  
1025 on the design of the LBNE 35 ton prototype, the MicroBooNE detector systems and the  
1026 current plans for the Long Baseline Far Detector.

1027 Main goal of the LAr system is to purge the cryostat prior to the start of the opera-

1028 tions (with GAr in open and closed loop), cool down the cryostat and fill it with LAr.  
 1029 Then continuously purify the LAr and the boil off GAr to maintain the required purity  
 1030 (electron lifetime measured by the detector).

1031 The LAr receiving facility includes a storage dewar and an ambient vaporizer to  
 1032 deliver LAr and GAr to the cryostat. The LAr goes through the liquid argon handling  
 1033 and purification system, whereas the Gar through the gaseous argon purification before  
 1034 entering the vessel.

1035 The LAr purification system is currently equipped with a filter containing mol sieve  
 1036 and copper beds, and a regeneration loop to regenerate the filter itself. Filters containing  
 1037 Oxsorb and Hydrosorb rather than mol sieve and copper beds, were also successfully  
 1038 employed. Same concept, but different medium. Studies are ongoing to standardize the  
 1039 filtration scheme and select the optimal filter medium for all future generation detectors,  
 1040 including this test prototype.

1041 During operation, an external LAr pump circulates the bulk of the cryogen through  
 1042 the LAr purification system. The boil off gas is first recondensed and then is sent to the  
 1043 LAr purification system before re-entering the vessel.

Table 9: Design requirements for the cryogenic system

Parameter	Value
Location	Preferably not in front of the cryostat (on the beam)
Cooling Power	TBD based on the heat leak of the cryostat (estimated 3.4 kW), the cryo-piping and all other contributions (cryogenic pumps, etc.)
Liquid argon purity in cryostat	10 ms electron lifetime (30 ppt O <sub>2</sub> equivalent)
Gaseous argon piston purge rate of rise	1.2 m/hr
Membrane cool-down rate	From manufacturer
TPCs cool-down rate	<40 K/hr, <10 K/m (vertically)
Mechanical load on TPC	The LAr or the gas pressure shall not apply a mechanical load to the TPC greater than 200 Pascal.
Nominal LAr purification flow rate (filling/ops)	5.5 day/volume exchange
Temperature of all surfaces in the ullage during operations	<100 K
Gaseous argon purge within insulation	1 volume change /day of the open space between insulation panels.
Lifetime of the cryogenic system	Consistent with the LAr program. TBD.

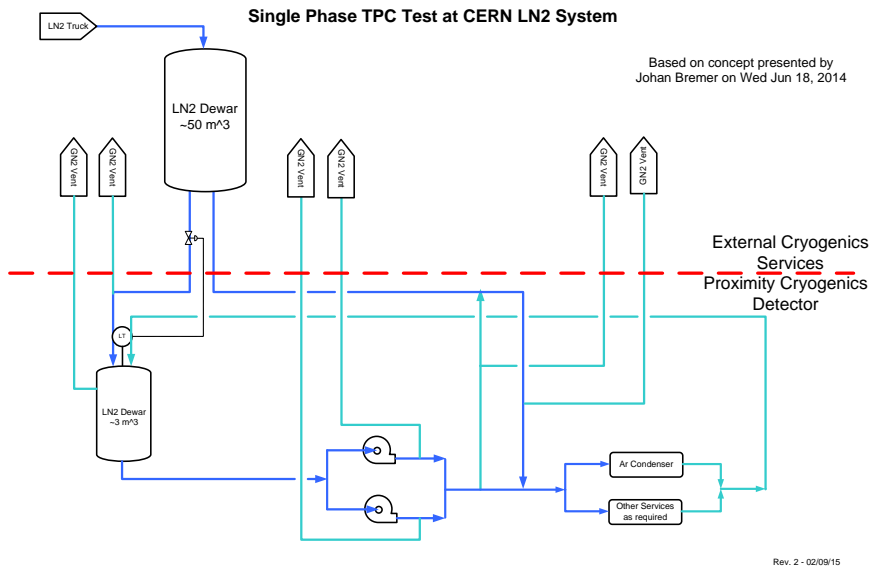


Figure 17: Schematic diagram for the proposed LN<sub>2</sub> system

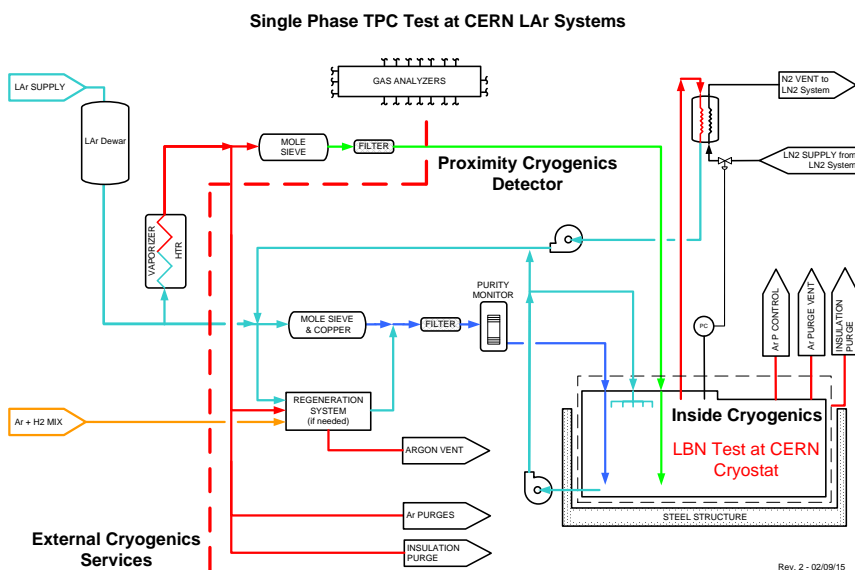


Figure 18: Schematic diagram for the proposed LAr system

1044 **5 Charged Particle Test Beam Requirements [ $\sim 10$**   
1045 **pages; Cheng-Ju]**

1046 **5.1 Particle Beam Requirements**

1047 The requested beam parameters are driven by the requirement that the results from the  
1048 CERN test beam should be directly applicable to the future large underground single-  
1049 phase LAr detector with minimal extrapolation. The CERN test beam data will be  
1050 used to evaluate the detector performance, to understand the various physics systematic  
1051 effects, and to provide “neutrino-like” data for event reconstruction studies. To satisfy  
1052 the requirement, the beam parameters must span a broad range of particle spectrum  
1053 that are expected in the future neutrino experiment. The particle beam composition  
1054 should consist of electrons, muons, and hadron beams that are charge-selected. The  
1055 expected momentum distributions for secondary particles from neutrino interactions are  
1056 shown earlier in Figure 2.1.1. There is a large spread in the momentum distribution with  
1057 most particles peaked near 200 MeV/c. To cover the momentum range of interest, the  
1058 momentum of the test beam should step from 0.1 GeV/c to 10 GeV/c. The maximum  
1059 electron drift time in the TPC is about 3 ms. To minimize pile-up in the TPC, the  
1060 desired beam rate should be around 200 Hz with the maximum rate below 300 Hz. The  
1061 single-phase TPC consists of two drift volumes. It is desirable to aim the particle beam  
1062 so that the hadronic showers are mostly contained in the same drift volume. However,  
1063 we also plan to take some data with hadronic shower crossing the midplane of the TPC  
1064 from one drift volume to another. The two beam entry angles and positions with respect  
1065 to the LAr cryostat are shown in Figures 19 and 20. The beam nominally enters the  
1066 cryostat slightly downward at an angle of about 6 degrees. Along the horizontal plane,  
1067 the beam enters the cryostat with an angle of 10 degrees. Another possible orientation  
1068 (not shown in the Figures) to study APA crossers is to reverse the angle of the beam  
1069 instead of shifting the beam parallel to the primary orientation. The summary of the  
1070 beam requirements are shown in Table 10.

Table 10: Particle beam requirements.

Parameter	Requirements	Notes
Particle Types	$e^\pm, \mu^\pm, \pi^\pm$	
Momentum Range	0.1 - 10 GeV/c	
Momentum Spread	$\Delta p/p < 5\%$	
Transverse Beam Size	RMS(x,y) < 2.5 cm	At the entrance face of the LAr cryostat
Beam Divergence		
Beam Angle (horizontal plane)	$\approx 10^\circ$	
Beam Dip Angle (vertical plane)	-6° (nominal); $\pm 5^\circ$ range	
Beam Entrance Position		
Rates	200 Hz (average); 300 Hz (maximum)	

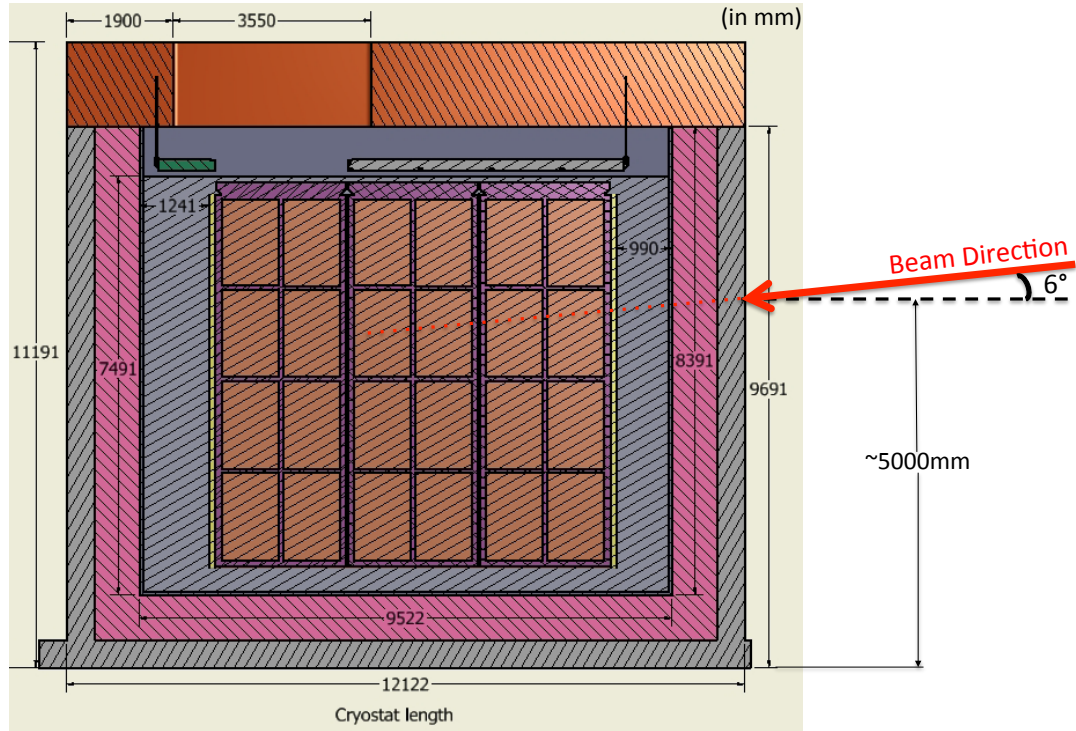


Figure 19: Side view: beam enters the cryostat slightly downward with a dip angle of 6 degrees.

## 1071 5.2 EHN1 H4ext Beamline

1072 The H4ext is an extension of the existing H4 beamline in Experimental Hall North 1  
1073 (EHN1). To produce particles in the momentum range of interest, 60 - 80 GeV/c pion  
1074 beam from the T2 target is used to generate tertiary beams. The tertiary particles are  
1075 momentum and charge-selected and transported down H4ext beamline to the experi-  
1076 mental area. A preliminary layout of the H4ext beamline is shown in Figure 21.

### 1077 5.2.1 Beam Optics

1078 [Waiting for inputs from Ilias]

### 1079 5.2.2 Expected Rates and Purity

1080 [Waiting for inputs from Ilias]

## 1081 5.3 Beam Instrumentation

1082 Beam instrumentation provides important information about the characteristics of the beam.  
1083 It is expected that a series of detectors will be installed along the beam line to  
1084 measure the particle momentum, identify particle type, and track the particle trajectory.

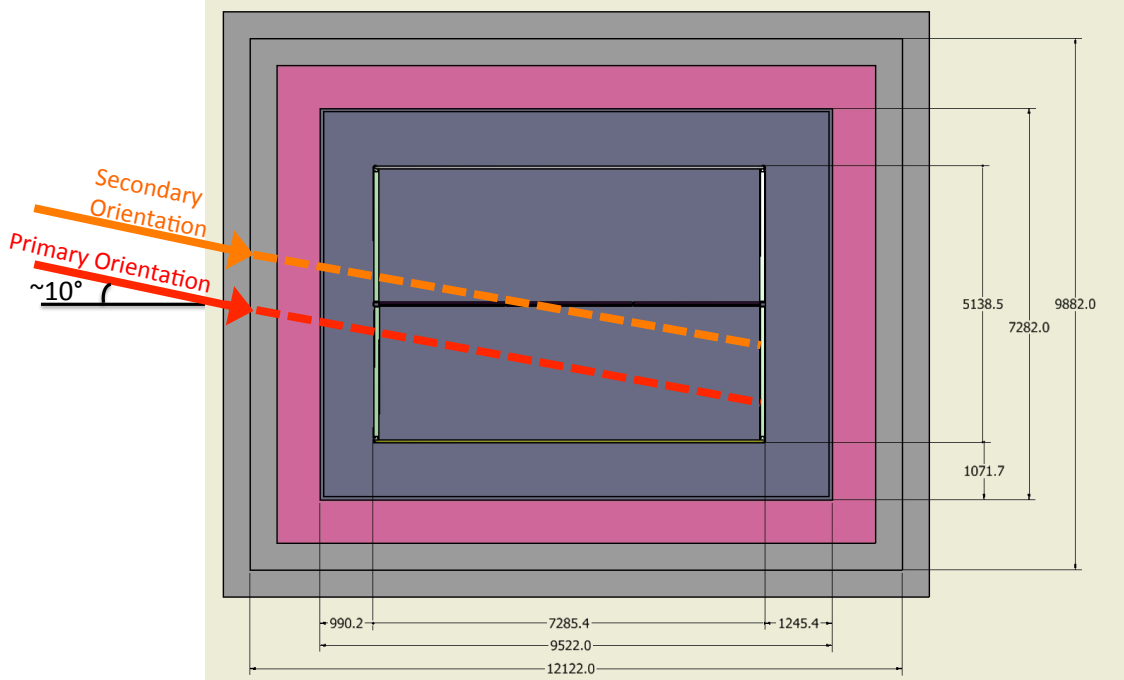


Figure 20: Top view: beam enters the cryostat with an entry angle of about 10 degrees along the horizontal plane. The primary orientation sends the particle beam into one TPC drift volume. The secondary orientation sends the particle beam across the APA.

### 1085 5.3.1 Beam Position Detector

1086 The beam position detector measures the positions of the particle as it traverses the  
1087 detector. Two detector technologies are under considerations: wire chambers and scin-  
1088 tillating fiber trackers. For the nominal setup, one beam position detector is installed  
1089 upstream and another one downstream of the last bending magnet. This pair provides  
1090 additional momentum information about the particles as well as the first set of posi-  
1091 tion measurements. A third detector is placed right in front of the beam window on  
1092 the cryostat wall to provide the last position information before the beam enters the  
1093 cryostat.

### 1094 5.3.2 Particle Identification

1095 In order to have good particle identification over large momentum range, two indepent  
1096 particle identification systems are needed in the beamline. The Time-of-Flight system  
1097 will be used to cover lower momentum range while a Threshold Cherenkov detector will  
1098 be tuned for higher momentum particles.

### 1099 5.3.3 Muon Beam Halo Counters

1100 The halo counter is a set of plastic scintillator paddles surrounding the beamline. The  
1101 main purpose is to tag particles (primarily muons from the upstream production target)  
1102 that are outside of the beam axis, but may potentially enter the TPC volume. The  
1103 counter information is used to either veto or simply flag these class of events.

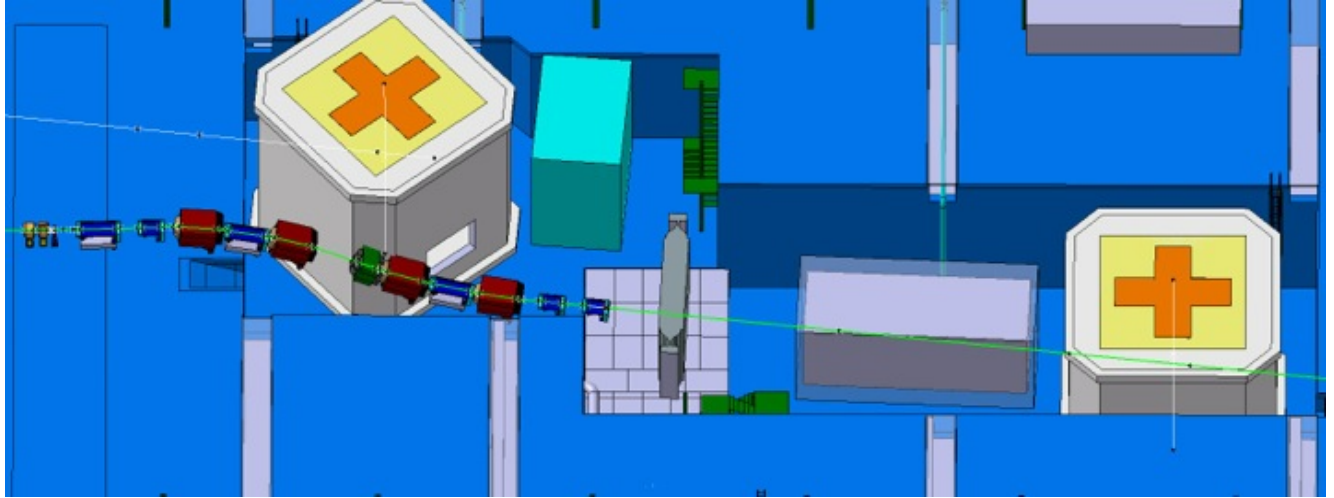


Figure 21: A conceptual layout of the H4ext beamline

#### **5.4 Beam Window on LAr Cryostat**

This section could be absorbed into the cryostat chapter.

## **6 Computing requirements, data handling and software [~3 pages; **Maxim/Craig**]**

The proposed “Full Scale” test of a single-phase Liquid Argon TPC at CERN will build upon the technology and expertise developed in the process of design and operation of its smaller predecessor, the 35t detector at FNAL. This includes elements of front-end electronics, data acquisition, run controls and related systems. We also expect that for the most part, Monte Carlo studies necessary to support this program will be conducted utilizing software evolved from tools currently used (2015).

In the test-beam setup, the detector performance will be characterized for different types of particles, e.g.  $p$ ,  $\pi^\pm$ ,  $\mu^\pm$  etc (see 2.1). Current plans call for measurements in pre-defined bins of the incident particle momentum, which will have widths ranging from tens to hundredths of MeV (see 6.1.3). The volume of data to be recorded shall be determined by the number of events to be collected in each measurement, such that it provides adequately low statistical uncertainty of the parameters measured.

In our view, it is optimal to first stage the “precious” data collected from the prototype on disk at CERN and then sink it to tape (also at CERN), while simultaneously performing replication to data centers in the US. For the latter, FNAL is the prime candidate, with additional data centers at Brookhaven National Laboratory and the NERSC facility as useful additional locations for better redundancy and more efficient access to the data from greater number of locations.

1126 **6.1 Collecting and Storing Raw Data**

1127 **6.1.1 Considerations for Event Size Estimates**

1128 To set the scale, let's consider an approximate **upper limit** on the number of channels  
1129 with signals above the threshold of zero-suppression, for a single track. For this we  
1130 assume digitization rate fixed at 2MHz, and 4312 samples per drift window. In a single  
1131 anode plane assembly (APA), it will be approximately of the order of channel count  
1132 in the APA, i.e. around 2500, *when the track is parallel to the APA plane*. Since each  
1133 sample is 16 bit (or 12 bit in more design), we arrive to the limit of approximately 20MB  
1134 per single charged track. For this class of events, the amount of data will scale roughly  
1135 linearly with the length of the track, i.e. in cases when a track is stopped or leaves  
1136 the sensitive volume there will be less data. Further, in most cases the data will be  
1137 zero-suppressed by the front-end electronics (e.g signals below a certain threshold will  
1138 not be included into the outgoing data stream). The exact data reduction factor will  
1139 depend on a variety of factors (cf. threshold), but as a rule of thumb it's an order of  
1140 magnitude. *We conclude therefore the events will typically be a few megabytes in size.*  
1141 This in fact is supported by previous Monte Carlo studies performed for earlier versions  
1142 of LBNE LAr TPC (more detail will be presented below).

1143 At the time of writing, work is being done on the physical design of the Liquid Argon  
1144 prototype, and the number of the Anode Plane Assemblies (APA) to be installed in the  
1145 detector is not yet finalized. It will likely be 2 or 3, however there is a possibility of this  
1146 number to be as high as 6. There is therefore a factor of two or three uncertainty in the  
1147 number of readout channels in the detector (e.g. 7680 with 3 APA vs 15360 with 6).

1148 This would affect the amount of data produced by DAQ, although not necessarily by  
1149 a factor of two since a large part of the raw data will be zero-suppressed and occupancy  
1150 in general is expected to be low. With each additional APA, the number of background  
1151 tracks (or track segments) produced by cosmic ray muons will scale very approximately  
1152 at a rate of  $O(1)$  per APA. Because of the direction of incidence of these tracks and  
1153 the fact that in most cases they will be crossing only part of the active volume, we will  
1154 account for this by adding data equivalent to approx. 5 extra tracks to each event. This  
1155 will very roughly correspond the upper limit of 6 APAs in the apparatus and thus the  
1156 estimate will be conservative.

1157 In addition to the principal sensitive volume where Liquid Argon will serve as active  
1158 medium for the TPC, the prototype will also contain a Photon Detector designed to  
1159 record light pulses produced in Argon due to scintillation caused by ionizing radiation.  
1160 In any realistic scenario, the amount of data to be produced by the Photon Detector will  
1161 be quite small compared to that of the Liquid Argon TPC. Same goes for other elements  
1162 of the experimental apparatus (hodoscopes, trigger systems etc) and as a result, for the  
1163 purposes of this section, we shall focus only on the Liquid Argon TPC as the critical  
1164 source of data.

1165 **6.1.2 “Before” and “After” Readout Windows**

1166 As we just mentioned, the detector will be sensitive to background tracks due to cosmic  
1167 ray particles. These must be properly identified and accounted for, in order to ensure  
1168 high quality of the measurements and subsequent detector characterization. Since over-

1169 lay of cosmic ray muons over beam events is stochastic in nature, the optimal way to  
1170 achieve this is by recording signals which were produced “just before” and “just after”  
1171 the arrival of the test particle from the beamline. This will enable us to reconstruct  
1172 either partial or complete background tracks present in the “main” event.

1173 To ensure complete collection of charge due to such tracks, the additional readout  
1174 windows before and after the beam event should equal the nominal total drift time for  
1175 the collection volume (approx. 2.1ms). This will triple the amount of data due to cosmic  
1176 rays, collected from the detector.

### 1177 6.1.3 Statistics and the Volume of Data

1178 Experimental program for the test includes triggering on a few types of particles over  
1179 a range of momenta (see 2.1). We introduce bins for the particle momenta as shown in  
1180 the table below. The estimated event sizes listed in the table are based on interpolation  
1181 of results from Monte Carlo studies performed earlier for the 10kt version of the LBNE  
1182 Far Detector and must be considered as approximate, ballpark estimates. Hadronic and  
1183 electromagnetic showers were included in the MC samples so their effect is accounted  
1184 for. As a concrete example, for an incident electron of 4GeV/c momentum calculations  
1185 indicate an average event size of ~2MB, after zero-suppression.

Particle Type	Momentum Range (GeV/c)	Bin (MeV/c)	Approx. event size, MB
$p$	0.1-2.0	100	1
$p$	2.0-10.0	200	5
$\mu^\pm$	0.1-1.0	50	1
$\mu^\pm$	1.0-10.0	200	5
$e^\pm$	0.1-2.0	100	1
$e^\pm$	2.0-10.0	200	4
$K^+$	0.1-1.0	100	1
$\gamma(\pi^0)$	0.1-2.0	100	1
$\gamma(\pi^0)$	2.0-5.0	200	5

1187 Preliminary plans call for statistics of the order of  $10^4 - 10^5$  events to be collected in  
1188 each bin. Depending on the assumptions, this translates into ~20 million events total  
1189 (for all event classes) to ensure enough statistics for subsequent analysis. Taking into  
1190 account the cosmic ray overlay and additional readout windows as explained in 6.1.2,  
1191 we arrive to a number of ~1PB for total storage space necessary to host **the raw data**.  
1192 This needs to be looked at as the basis for tape budget. As explained below, this volume  
1193 of data needs to be replicated for assured preservation, in at least one more additional  
1194 facility, hence in effect this number must be doubled when budgeting tape.

### 1195 6.1.4 Summary of the Data Volume Estimates

1196 The total amount of data to be collected during the prototype operation will be con-  
1197 siderable under all assumptions and estimates. To fulfill the mission of this test beam  
1198 experiment, we expect that we will need tape storage of  $O(PB)$  size, and a more modest  
1199 disk space for raw data staging at CERN, for replication purposes. We envisage storing

1200 the primary copy of raw data at CERN, with replicas at additional locations. There will  
1201 be additional requirements for processed and Monte Carlo data placement.

### 1202 **6.1.5 Raw Data Transmission and Distribution**

1203 Moving data to remote locations outside of CERN is subject to a number of requirements  
1204 that include:

- 1205     ● automation
- 1206     ● monitoring
- 1207     ● error checking and recovery (redundant checks to ensure the “precious” data was  
1208       successfully sunk to mass storage at the endpoint)
- 1209     ● compatibility with lower-level protocols that are widespread, well understood and  
1210       maintained (cf. gridFTP)

1211 There are a number of systems that can satisfy these requirements, and one of them  
1212 where we possess sufficient expertise and experience is Spade, first used in IceCube [1]  
1213 and then enhanced and successfully utilized in Daya Bay experiment [2].

## 1214 **6.2 Databases**

1215 A few types of databases will be required for the test:

- 1216     ● Run Log, Conditions and Slow Controls records
- 1217     ● Offline Calibrations

1218 Database servers listed in the former item will need to be local to the experiment  
1219 (i.e. at CERN) in order to reduce latency, improve reliability, reduce downtime due to  
1220 network outages etc. A replication mechanism will need to be put in place the data is  
1221 readily available at the US and other sites. The volume of data stored in these databases  
1222 will likely to be quite modest.

## 1223 **6.3 A note on Simulation and Reconstruction Software**

1224 Research effort connected to the “Full Scale” prototype at CERN will benefit from  
1225 utilizing simulation toolkits, and tracking and other reconstruction algorithms created  
1226 by communities such as former LBNE, and especially during the 35t test at FNAL.

1227 *In order to leverage this software and expertise, appropriate manpower will need to  
1228 be allocated in order to create and maintain physics analysis tools necessary to fulfill the  
1229 research goals of this experiment.* Given the widely distributed nature of the Collabora-  
1230 tion and the need to use geographically dispersed resources (see 6.4.1, the software  
1231 components of these tools will need to be portable, well maintained and validated. To  
1232 ensure that this happens, we plan to establish close cooperation among participating  
1233 laboratories and other research institutions.

1234 **6.4 Distributed Computing, Workload and Workflow Management**  
1235

1236 **6.4.1 Distributed Processing**

1237 At the time of writing, FNAL provides the bulk of computational power for LBNE (not  
1238 to mention a few other IF experiments), via Fermigrid and other facilities. We plan to  
1239 leverage these resources to process the data coming from the test.

1240 Given the relatively limited amount of beam time for this test, one of the principal  
1241 goals will be quick validation of the data collected in each measurement, in order to be  
1242 able to make adjustments during the run as necessary. This is a common practice in  
1243 other experiment which have "express streams" to assess data quality (cf. [3]).

1244 There are currently very large uncertainties regarding what scale of CPU power will  
1245 be required to process the data, given that tracking, reconstruction and other algorithms  
1246 are in a fairly early stage of development. The estimates we have at this point range  
1247 from 10 to 100 seconds required by a typical CPU to reconstruct a single event. This  
1248 means that utilizing a few thousand cores through Grid facilities, it will be possible to  
1249 ensure timely processing of these data.

1250 To ensure adequate capacity, we envisage a distributed computing model where Grid  
1251 resources are utilized in addition to FNAL. As an example, we have had good experience  
1252 working with the Open Science Grid Consortium.

1253 **6.4.2 Scale of the Processed Data**

1254 As discussed above, we estimat the volume of raw data to be in the petabyte range. We  
1255 also must address the offline data, which can be classified as follows:

- 1256 • Monte Carlo data, which will contain multiple event samples to cover various event  
1257 types and other conditions during the measurements with the prototype detector
- 1258 • Data derived from Monte Carlo events, and produced with a variety of tracking  
1259 and pattern recognition algorithms in order to create a basis for the detector  
1260 characterization
- 1261 • Intermediate calibration files, derived from calibration data
- 1262 • Processed experimental data, which will likely exist in a few brunches correspond-  
1263 ing to a few reconstruction algorithms being applied, with the purpose of their  
1264 evaluation

1265 In the latter, there will likely be more than one processing step, thus multiplying  
1266 data volume. There is sometimes a question about how much of the raw data should be  
1267 preserved in the processed data streams. Given a relatively large volume of raw data, the  
1268 answer in this case will likely be "none" - for practical reasons, meaning that the derived  
1269 data will be just that, and that the size of the processed data will likely by significantly  
1270 smaller than the input (the raw data). Given consideration presented above, we will  
1271 plan for  $\sim$ 1PB of tape storage to keep the processed data. For efficient processing, disk  
1272 storage will be necessaty to stage a considerable portion of both raw data (inputs) and  
1273 one or a few steps in processing (outputs).

1274     Extrapolating from our previous experience running Monte Carlo for the former  
1275     LBNE Far Detector, we estimate that we'll need a few hundred TB of continuously  
1276     available disk space. In summary, we request 2PB of disk storage at FNAL to ensure  
1277     optimal data availability and processing efficiency. Access to distributed data is discussed  
1278     below.

#### 1279     **6.4.3 Distributed Data**

1280     We foresee that data analysis (both experimental data and Monte Carlo) will be per-  
1281     formed by collaborators residing in many institutions and geographically dispersed. In  
1282     our estimated above, we mostly outlined storage space requirements for major data  
1283     centers like CERN and FNAL. When it comes to making these data available to the  
1284     researchers, we will utilize a combination of the following:

- 1285         • Managed replication of data in bulk, performed with tools like Spade discussed  
1286         above. Copies will be made according to wishes and capabilities of participating  
1287         institutions.
- 1288         • Network-centric federated storage, based on XRootD. This allows for agile, just-  
1289         in-time delivery of data to worker nodes and workstations over the network. This  
1290         technology has been evolving rapidly in the past few years, and solutions have been  
1291         found to mitigate performance penalty due to remote data access, by implementing  
1292         caching and other techniques.

1293     In order to act on the latter item, we plan to implement a global XRootD redirector,  
1294     which will make it possible to transparently access data from anywhere. A concrete  
1295     technical feature of storage at FNAL is that there is a dCache network running at this  
1296     facility, with substantial capacity which can be leveraged for the needs of the CERN  
1297     prototype analysis. This dCache instance is equipped with a XRootD “door” which  
1298     makes it accessible to outside world, subject to proper configuration, authentication and  
1299     authorization.

1300     As already mentioned, we plan to host copies of a significant portion of raw and  
1301     derived data at NERSC and also at Brookhaven National Laboratory. These two insti-  
1302     tutions have substantial expertise in the field of data handling and processing at scale  
1303     and will serve as “hubs” for data archival and distribution.

## 1304     **7 CERN neutrino platform test environment [5 pages;** 1305     **David/Jack/Cheng-Ju/Thomas]**

1306     Description of Requirements, layout and constraints

1307     We propose that the cryostat be housed in the extension of the EHN1 Bat 887 at  
1308     CERN, where the cryogenic system components will also be located. (moved to sec 7)

- 1309         • short description of location and orientation of cryostat + cryogenics system in  
1310         EHN1 (David)
- 1311         • description of beam line layout (Cheng-Ju)

- 1312     ● space for staging, control room, electronics racks, clean room, scaffolding, etc.  
 1313        (Jack)
- 1314     ● power requirements and cooling (Jack ?)
- 1315     ● ...

1316   **8 Schedule, organization and cost estimate [~5 pages;**  
 1317       **Thomas/Greg]**

1318   **8.1 Schedule**

1319   The schedule of the proposed CERN prototype detector and beam test is dictated by  
 1320   the ELBNF overall schedule which foresees to place the first 10 kton detector module  
 1321   underground as early as calendar year 2021. Additional detector modules are expected to  
 1322   follow shortly thereafter. Ideally information and results from the CERN beam test will  
 1323   inform the decision about the final ELBNF detector design and hence should be available  
 1324   as soon as realistically possible. In addition, the LHC long shutdown, which is presently  
 1325   scheduled for mid-2018 represents a significant constraints on the schedule. In order  
 1326   to meet the first requirement, data taking for the initial measurement program should  
 1327   be complete prior to the long LHC shutdown in mid-2018. Figure 22 shows a schedule  
 1328   which meets this requirement. The shown schedule is based on experience of designing  
 1329   and manufacturing components for the 35t detector which will be commissioned starting  
 in June 2015 at Fermilab.

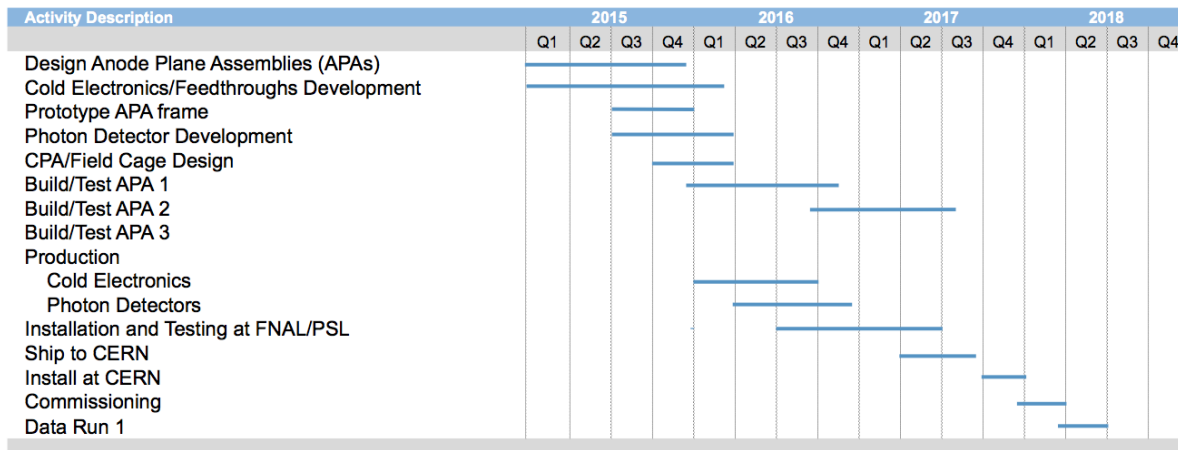


Figure 22: Rolled up version of a draft schedule for manufacturing, installing and commissioning the CERN prototype detector. A 2 - 3 months data taking period is included in the schedule.

1330

1331   **8.2 Organization**

- 1332     ● working group structure and distributions of tasks/responsibilities

<sub>1333</sub> **8.3 Division of Responsibilities**

<sub>1334</sub> **8.3.1 Shared responsibilities**

<sub>1335</sub> The engineering design of the cryostat and the cryogenics system is considered to be a  
<sub>1336</sub> shared responsibility between ELBNF and CERN.

<sub>1337</sub> **8.3.2 ELBNF responsibilities**

<sub>1338</sub> The following detector components are expected to be covered by ELBNF project:

<sub>1339</sub> 1. XX APAs

<sub>1340</sub> 2. CPA

<sub>1341</sub> 3. field cage

<sub>1342</sub> 4. cold electronics

<sub>1343</sub> 5. DAQ hardware and software

<sub>1344</sub> 6. ...

<sub>1345</sub> **8.3.3 CERN responsibilities**

<sub>1346</sub> **The beam line** design, setup of the beam line and beam monitoring instrumentation  
<sub>1347</sub> are expected to be provided by CERN.

<sub>1348</sub> **The cryostat and cryogenics system** are expected to be organized and paid for  
<sub>1349</sub> by the CERN nu-platform. The scope of the EHN1 cryostat subsystem includes the  
<sub>1350</sub> design, procurement, fabrication, testing, delivery and oversight of a cryostat to contain  
<sub>1351</sub> the liquid argon and the TPC.

<sub>1352</sub>  
<sub>1353</sub> The following items (incomplete list !) require further discussion. The responsibilities  
<sub>1354</sub> should be clearly spelled out.

<sub>1355</sub> • plans for data analysis and publications

<sub>1356</sub> • describe overlap/commonalities with WA105 data analysis

<sub>1357</sub> **9 Summary [~2 pages; Thomas/Greg]**

<sub>1358</sub> this is the summary section

1359 **References**

- 1360 [1] IceCube Data Movement [https://icecube.wisc.edu/science/data/  
1361 datamovement](https://icecube.wisc.edu/science/data/datamovement).
- 1362 [2] Data processing and storage in the Daya Bay Reactor Antineutrino Experiment  
1363 <http://arxiv.org/pdf/1501.06969.pdf>.
- 1364 [3] Prompt reconstruction of LHC collision data with the ATLAS reconstruction soft-  
1365 ware, N.Barlow et al, *Journal of Physics: Conference Series* 331 (2011) 032004
- 1366 [4] First scientific application of the membrane cryostat technology, D.Montanari et al,  
1367 *AIP Proceedings* 1573, 1664 (2014) [http://scitation.aip.org/content/aip/  
1368 proceeding/aipcp/10.1063/1.4860907](http://scitation.aip.org/content/aip/proceeding/aipcp/10.1063/1.4860907)
- 1369 [5] A Proposal for a Three Detector Short-Baseline Neutrino Oscillation Program in the  
1370 Fermilab Booster Neutrino Beam *R.Acciarri et al* [http://arxiv.org/abs/1503.  
1371 01520](http://arxiv.org/abs/1503.01520)

1372 → total estimated page count: ~60 pages